

Characterization of the interface between normal and transformed epithelial cells

Catherine Hogan¹, Sophie Dupré-Crochet^{1,7}, Mark Norman¹, Mihoko Kajita¹, Carola Zimmermann¹, Andrew E. Pelling³, Eugenia Piddini⁴, Luis Alberto Baena-López⁴, Jean-Paul Vincent⁴, Yoshifumi Itoh⁵, Hiroshi Hosoya⁶, Franck Pichaud^{1,2} and Yasuyuki Fujita^{1,2,8}

In most cancers, transformation begins in a single cell in an epithelial cell sheet^{1–3}. However, it is not known what happens at the interface between non-transformed (normal) and transformed cells once the initial transformation has occurred. Using Madin-Darby canine kidney (MDCK) epithelial cells that express constitutively active, oncogenic Ras (Ras^{V12}) in a tetracycline-inducible system, we investigated the cellular processes arising at the interface between normal and transformed cells. We show that two independent phenomena occur in a non-cell-autonomous manner: when surrounded by normal cells, Ras^{V12} cells are either apically extruded from the monolayer, or form dynamic basal protrusions and invade the basal matrix. Neither apical extrusion nor basal protrusion formation is observed when Ras^{V12} cells are surrounded by other Ras^{V12} cells. We show that Cdc42 and ROCK (also known as Rho kinase) have vital roles in these processes. We also demonstrate that *E-cadherin* knockdown in normal cells surrounding Ras^{V12} cells reduces the frequency of apical extrusion, while promoting basal protrusion formation and invasion. These results indicate that Ras^{V12}-transformed cells are able to recognize differences between normal and transformed cells, and consequently leave epithelial sheets either apically or basally, in a cell-context-dependent manner.

Cell transformation arises from the activation of oncproteins and/or inactivation of tumour suppressor proteins¹. During the initial stage of carcinogenesis, transformation occurs in a single cell in an epithelial monolayer^{2,3}. However, it remains unclear what happens at the interface between normal and transformed cells during this process. For example, do surrounding normal cells recognize the transformation that has occurred in their neighbour? What is the fate of the transformed cell when surrounded by normal cells? To address these questions, we

established MDCK epithelial cells expressing GFP-tagged Ras^{V12} in a tetracycline-inducible manner (MDCK-pTR GFP-Ras^{V12}; Supplementary Information, Fig. S1a, b). After addition of tetracycline to cells plated at low density, expression of GFP-Ras^{V12} induced cell scattering and downregulation of cell–cell contacts (Supplementary Information, Fig. S1c)⁴. In contrast, when cells were plated at high density, expression of GFP-Ras^{V12} did not induce loss of cell–cell adhesion, and cells retained an epithelial morphology (Supplementary Information, Fig. S1d). In all subsequent experiments, we cultured cells at high density.

To examine the fate of a single Ras^{V12} cell in a monolayer of normal MDCK cells, MDCK-pTR GFP-Ras^{V12} cells were labelled with fluorescent dye (CMPTX) and mixed with normal MDCK cells at a ratio of 1:100. The combination of cells was then cultured on a collagen matrix in the absence of tetracycline until a monolayer was formed. Subsequently, GFP-Ras^{V12} expression was induced with tetracycline, and the fate of Ras^{V12} cells surrounded by normal cells was observed using time-lapse microscopy. Between 13 and 25 h after tetracycline addition, Ras^{V12} cells were frequently extruded from the apical surface of the monolayer (84% of tracked cells, $n = 74$; Fig. 1a; Supplementary Information, Movie 1). We observed that Ras^{V12} cells often underwent cell division before extrusion; however, we also observed extrusion of single Ras^{V12} cells (Supplementary Information, Fig. S2a). After extrusion, Ras^{V12} cells continued to proliferate and form multicellular aggregates (Fig. 1a, c; Supplementary Information, Movie 1). These multicellular structures attached loosely to the underlying normal cells and dynamically moved over them (Supplementary Information, Fig. S2b and Movie 1). Extruded Ras^{V12} cells did not stain with ethidium dye (data not shown), indicating that they remained alive. Treatment with the K⁺ channel inhibitor 4-aminopyridine (4-AP), which blocks the early stage of apoptosis in epithelial cells⁵, did not appreciably reduce the frequency of extrusion (Fig. 1d), further indicating that extrusion of Ras^{V12} cells occurs in a cell death-independent manner. Cells expressing

¹MRC Laboratory for Molecular Cell Biology and Cell Biology Unit, ²Department of Cell and Developmental Biology, University College London, Gower Street, London, WC1E 6BT, UK. ³London Centre for Nanotechnology and Centre for Nanomedicine, 17–19 Gordon Street, London, WC1H 0AH, UK. ⁴Division of Developmental Neurobiology, National Institute for Medical Research, London, NW7 1AA, UK. ⁵Imperial College London, The Kennedy Institute of Rheumatology, 1 Aspenlea Road, London, W6 8LH, UK. ⁶Department of Biological Science, Graduate School of Science, Hiroshima University, Higashi-Hiroshima 739–8526, Japan. ⁷Current address: INSERM UMR 757, Université Paris-sud, Bat 443, 91405 Orsay cedex, France.

⁸Correspondence should be addressed to Y.F. (e-mail: y.fujita@ucl.ac.uk)

Received 30 October 2008; accepted 12 December 2008; published online 15 March 2009; DOI: 10.1038/ncb1853

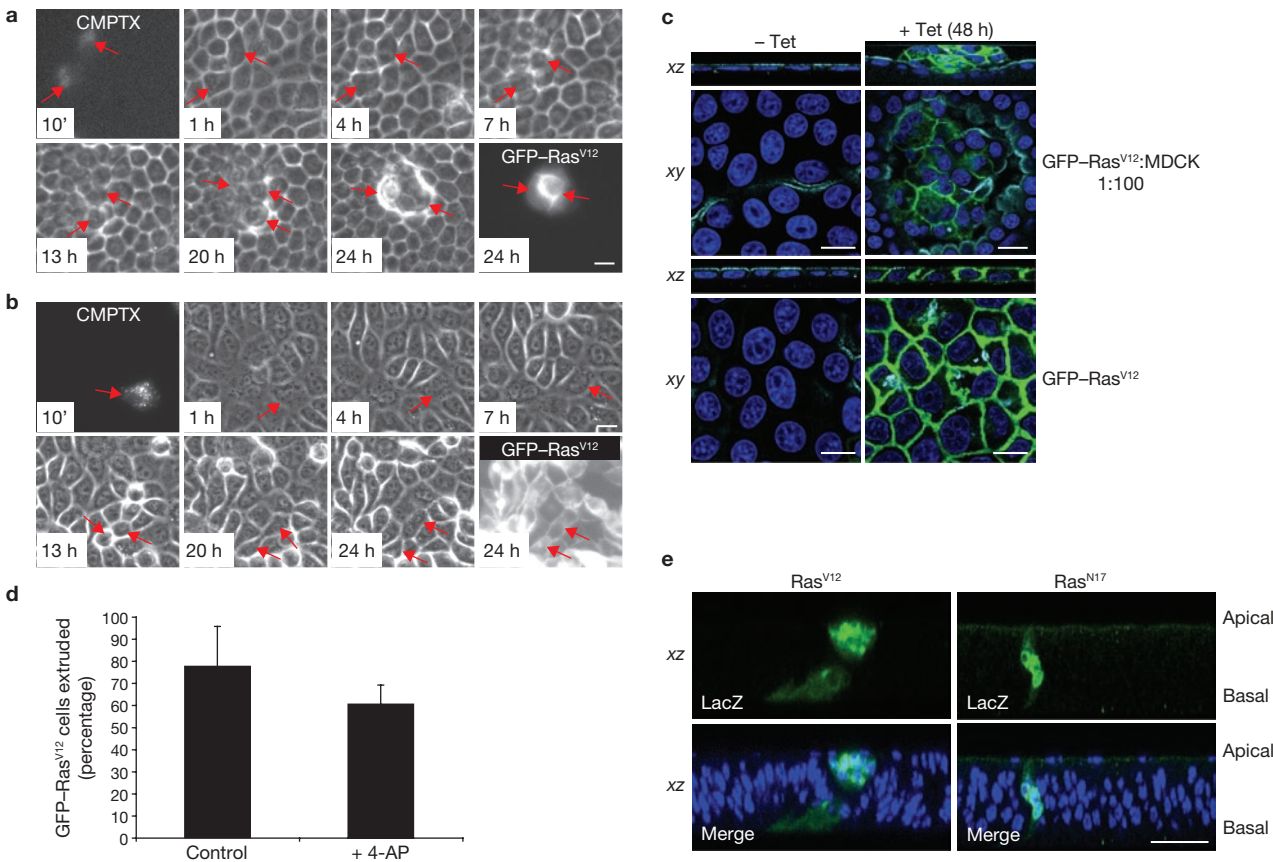


Figure 1 Epithelial cells expressing Ras^{V12} are apically extruded from surrounding normal epithelium in a non-cell-autonomous manner. **(a, b)** Ras^{V12}-expressing cells were extruded from a monolayer of normal cells, but not from a monolayer of Ras^{V12}-expressing cells. MDCK-pTR GFP-Ras^{V12} cells were combined with normal MDCK cells **(a)** or MDCK-pTR GFP-Ras^{V12} cells **(b)** at a ratio of 1:100 and cultured on type-I collagen gels, followed by tetracycline treatment. Images were extracted from a representative time-lapse analysis. Red arrows indicate fluorescently labelled Ras^{V12} cells. **(c)** Confocal images of xz and xy sections of GFP-Ras^{V12} cells combined with normal MDCK cells (upper panels) or

GFP-Rap1^{V12}, a constitutively active form of Ras-related non-oncogenic small GTPase⁶, were not extruded but remained in the monolayer of normal cells (Supplementary Information, Fig. S2c, d and Movie 2). In the absence of tetracycline, we did not observe extrusion of Ras^{V12} cells (data not shown). Moreover, fluorescently labelled Ras^{V12} cells were not extruded when mixed with non-labelled Ras^{V12} cells (Fig. 1b, c; Supplementary Information, Movie 3), suggesting that the extrusion of Ras^{V12} cells depends on their interaction with normal cells. Similarly, fluorescently labelled normal cells were not extruded from a monolayer of normal cells (data not shown). Taken together, these data indicate that the extrusion of Ras^{V12} cells occurs in a non-cell-autonomous manner only when they are surrounded by normal cells. To examine the physiological relevance of this observation, Ras^{V12} was expressed in a mosaic manner in wing imaginal discs of *Drosophila melanogaster*. Ras^{V12}-expressing cells were apically extruded from normal epithelial cell sheets (14%, n = 85; Fig. 1e, left panels), showing that apical extrusion of Ras^{V12}-expressing cells occurs *in vivo*. Cells expressing Ras^{N17}, a constitutively inactive form of Ras, or wild-type Ras were not extruded and remained within the disc epithelium (0%, n = 28 or 0%, n = 19;

with GFP-Ras^{V12} cells (lower panels) on collagen gels. Cells were fixed after 48 h incubation with (+ Tet, 2 µg ml⁻¹) or without (- Tet) tetracycline and stained with anti-gp135 antibody (cyan) and Hoechst (blue). **(d)** Quantification of time-lapse analyses of Ras^{V12} cells extruded from a monolayer of normal cells 24 h after tetracycline addition in the absence (control) or presence of 4-AP. Data are mean ± s.d. of three independent experiments (n = 98 cells control, n = 101 cells 4-AP). **(e)** *Drosophila* wing imaginal disc epithelium co-expressing lacZ and Ras^{V12} or Ras^{N17}. Cells were stained with anti-β-galactosidase antibody (green) and Hoechst (blue). Scale bars, 20 µm (**a–c, e**).

Fig. 1e, right panels; Supplementary Information, Fig. S3a). When Ras^{V12} was expressed in the entire epithelium, the monolayer became irregularly folded but we did not observe apical extrusion (Supplementary Information, Fig. S3b)⁷.

To understand the molecular mechanism of apical extrusion, we analysed Ras^{V12}-expressing MDCK cells that were not yet extruded and remained in the monolayer of normal MDCK cells. We found that the height of Ras^{V12} cells along the apicobasal axis was significantly higher than that of the surrounding normal cells (Fig. 2a, b). When Ras^{V12} cells alone formed a monolayer, the cell height was comparable to that of normal cells (Fig. 2b). These results indicate that the height of Ras^{V12} cells increases in a cell-context-dependent manner. We also observed that phosphorylation of myosin light chain was enhanced in Ras^{V12} cells with increased height (Fig. 2c), but not in those with similar height to surrounding normal cells (data not shown), suggesting a correlation between increased cell height and activation of myosin. Furthermore, we found that F-actin accumulated at cell-cell contacts between Ras^{V12} cells surrounded by normal cells (Fig. 2a, d), but not when surrounded by Ras^{V12} cells (Fig. 2d). F-actin did not accumulate between normal

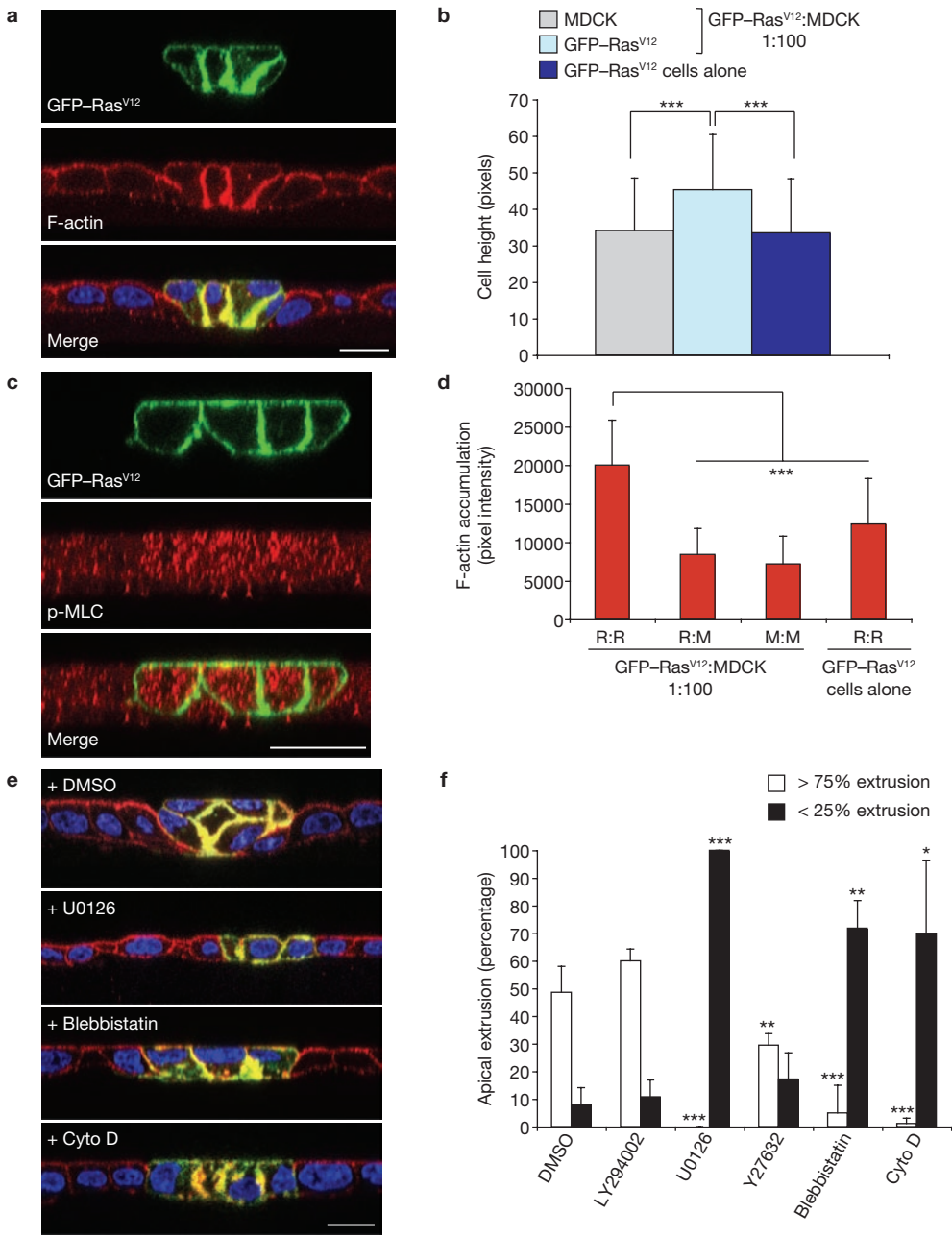


Figure 2. Molecular mechanism for apical extrusion of Ras^{V12}-expressing cells from a monolayer of normal cells. **(a)** Confocal images of xz sections of MDCK-pTR GFP-Ras^{V12} cells in a monolayer of normal MDCK cells. Twenty-four hours after tetracycline addition, cells were stained with TRITC-phalloidin (red) and Hoechst (blue). **(b)** Quantification of cell height. Grey bar, MDCK cells ($n = 155$); light blue bar, GFP-Ras^{V12} cells surrounded by MDCK cells ($n = 103$); dark blue bar, GFP-Ras^{V12} cells only ($n = 177$). Data are mean \pm s.d.; *** $P < 0.0001$; n , cells. A total of 40–85 cells from three independent experiments were analysed. **(c)** Enhanced phosphorylation of myosin light chain (p-MLC) in GFP-Ras^{V12} cells surrounded by normal cells. Twenty hours after tetracycline addition, cells were stained with anti-phospho-MLC antibody (red). **(d)** Quantification of F-actin accumulation at cell–cell contacts. R:R, between Ras^{V12} cells (with normal cells $n = 38$, Ras^{V12} cells alone $n = 64$); R:M, between Ras^{V12} and normal MDCK cells

and Ras^{V12} cells (Fig. 2a, d). Collectively, these results suggest that Ras^{V12} cells recognize that they are surrounded by normal cells and modulate their shape and cytoskeleton accordingly. E-cadherin-based cell–cell

($n = 24$); M:M, between normal MDCK cells ($n = 52$). Data are mean \pm s.d.; *** $P < 0.0001$; n , cell–cell contacts. **(e)** GFP-Ras^{V12} cells in a monolayer of normal MDCK cells after treatment with inhibitors. Twenty-four hours after tetracycline addition in the presence of U0126, blebbistatin or cytochalasin D (Cyto D), cells were stained with TRITC-phalloidin (red) and Hoechst (blue). Merged images are shown. **(f)** Quantification of frequency of apical extrusion of GFP-Ras^{V12} cells from a monolayer of MDCK cells in the presence of various inhibitors. In each experiment, approximately 20 groups of Ras^{V12}-expressing cells were counted. White bar, more than 75% of cells in a group of Ras^{V12} cells are apically extruded. Black bar, less than 25% of cells are extruded. Data are mean \pm s.d. of at least four independent experiments; *** $P < 0.0001$, ** $P < 0.005$, * $P < 0.05$; $n = 123, 57, 76, 55, 52$ and 57 groups of cells, for each inhibitor, respectively. Scale bars, 20 μm (a, c, e).

contacts between Ras^{V12} cells were not disrupted when these cells were in the monolayer of normal cells (Supplementary Information, Fig. S4a), or after they were apically extruded (data not shown), suggesting that

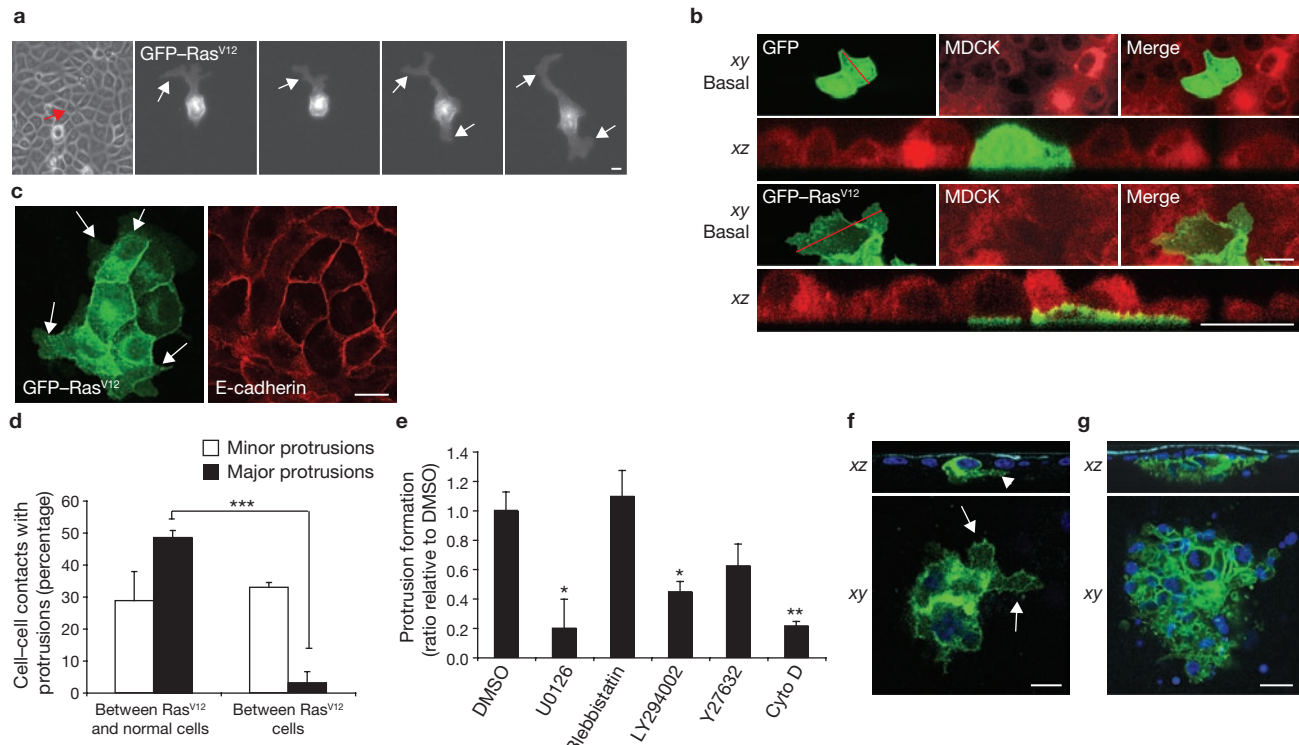


Figure 3. Non-extruded GFP–Ras^{V12} cells produce dynamic basal protrusions beneath the neighbouring MDCK cells. **(a)** Images extracted from a time-lapse analysis of a GFP–Ras^{V12} cell (red arrow) surrounded by normal cells. Images were captured at 50 min intervals. White arrows indicate protrusions. **(b)** Confocal images of MDCK cells expressing GFP (upper panels) or GFP–Ras^{V12} (lower panels) in a monolayer of normal cells. Red bars in the xy-labelled panels denote the cross-sections represented in xz labelled panels. Surrounding normal cells were labelled with CMPTX (red). **(c)** Confocal images of GFP–Ras^{V12} cells in a monolayer of normal cells stained with anti-E-cadherin antibody (red, right panel). White arrows indicate protrusions. **(d)** Quantification of protrusion formation at cell–cell

deregulation of E-cadherin in Ras^{V12} cells is not involved in apical extrusion. To further investigate the molecular mechanism of apical extrusion of Ras^{V12} cells, we examined the effect of various inhibitors that modulate cell signalling and/or the cytoskeleton. Among the signalling pathways downstream of active Ras, the mitogen-activated protein kinase (MAPK) and phosphatidylinositol-3-kinase (PI(3)K) pathways are required for Ras-induced transformation⁸. Addition of U0126, an inhibitor of MAPK kinases, completely suppressed apical extrusion of Ras^{V12} cells, whereas the PI(3)K inhibitor LY294002 had no effect (Fig. 2e, f), suggesting that the MAPK pathway is involved in apical extrusion. As PI(3)K has been shown to have a crucial role in lamellipodia formation⁹, it is unlikely that apical extrusion is due to increased migration of Ras^{V12} cells. Indeed, we never observed lamellipodia or membrane ruffling of Ras^{V12} cells during or after extrusion (data not shown). Blebbistatin and cytochalasin D, which inhibit myosin-II activity and actin polymerization respectively, significantly suppressed apical extrusion (Fig. 2e, f), as did the ROCK inhibitor Y27632 (Fig. 2f). Blebbistatin also suppressed the increase in cell height of Ras^{V12} cells surrounded by normal cells (data not shown). Taken together, these data indicate that myosin-II activity and actin polymerization are required for apical extrusion of Ras^{V12} cells.

Although most Ras^{V12} cells were apically extruded when surrounded by normal cells, we also observed Ras^{V12} cells that were not extruded.

contacts between Ras^{V12} and normal cells ($n = 230$) or between Ras^{V12} cells ($n = 180$). Data are mean \pm s.d.; *** $P < 0.0001$; n , cell–cell contacts. **(e)** Quantification of protrusion formation of GFP–Ras^{V12} cells in a monolayer of normal cells in the presence of various inhibitors. Values are expressed as a ratio relative to the DMSO control, and represent mean \pm s.e.m.; * $P < 0.05$ ** $P < 0.005$; $n = 320, 170, 300, 382, 362$ and 40 groups of cells, for each inhibitor, respectively. **(f)**, **(g)** Confocal images of GFP–Ras^{V12} cells in a monolayer of normal MDCK cells on collagen gels. After (f) 48 h or (g) 120 h of tetracycline incubation, cells were stained with anti-gp135 antibody (cyan) and Hoechst (blue). White arrows and arrowhead indicate protrusions. Scale bars, 20 μm (a–c, f, g).

We examined the fate of these non-extruded cells, and found that non-extruded Ras^{V12} cells formed large protrusions that dynamically extended and retracted, often over distances of several cell diameters (Fig. 3a; Supplementary Information, Movie 4). Confocal microscopy analysis, showed that these protrusions extended beneath the neighbouring normal cells (Fig. 3b, lower panels). In contrast, MDCK cells expressing GFP did not produce large protrusions (Fig. 3b, upper panels). Apical extrusion and basal protrusion formation of Ras^{V12} cells were observed in the same monolayer of normal cells (Supplementary Information, Fig. S4b). When expression of Ras^{V12} was induced in a group of cells within a monolayer of normal cells, major protrusions ($> 10 \mu\text{m}$) were frequently formed at the interface between Ras^{V12} and normal cells (Fig. 3c, white arrows, 3d), but were rarely observed between Ras^{V12} cells (Fig. 3c, d). This indicates that protrusion formation also occurs in a non-cell-autonomous fashion. Both F-actin and microtubules were found within the protrusions (Supplementary Information, Fig. S4c), suggesting a role for the cytoskeleton in the dynamic movement of protrusions. Although blebbistatin inhibited apical extrusion (Fig. 2f), it did not affect protrusion formation (Fig. 3e). In contrast, LY294002 inhibited protrusion formation (Fig. 3e), but not apical extrusion (Fig. 2f). Therefore, apical extrusion and basal protrusion formation are regulated, at least partially, by distinct molecular mechanisms. We also found that

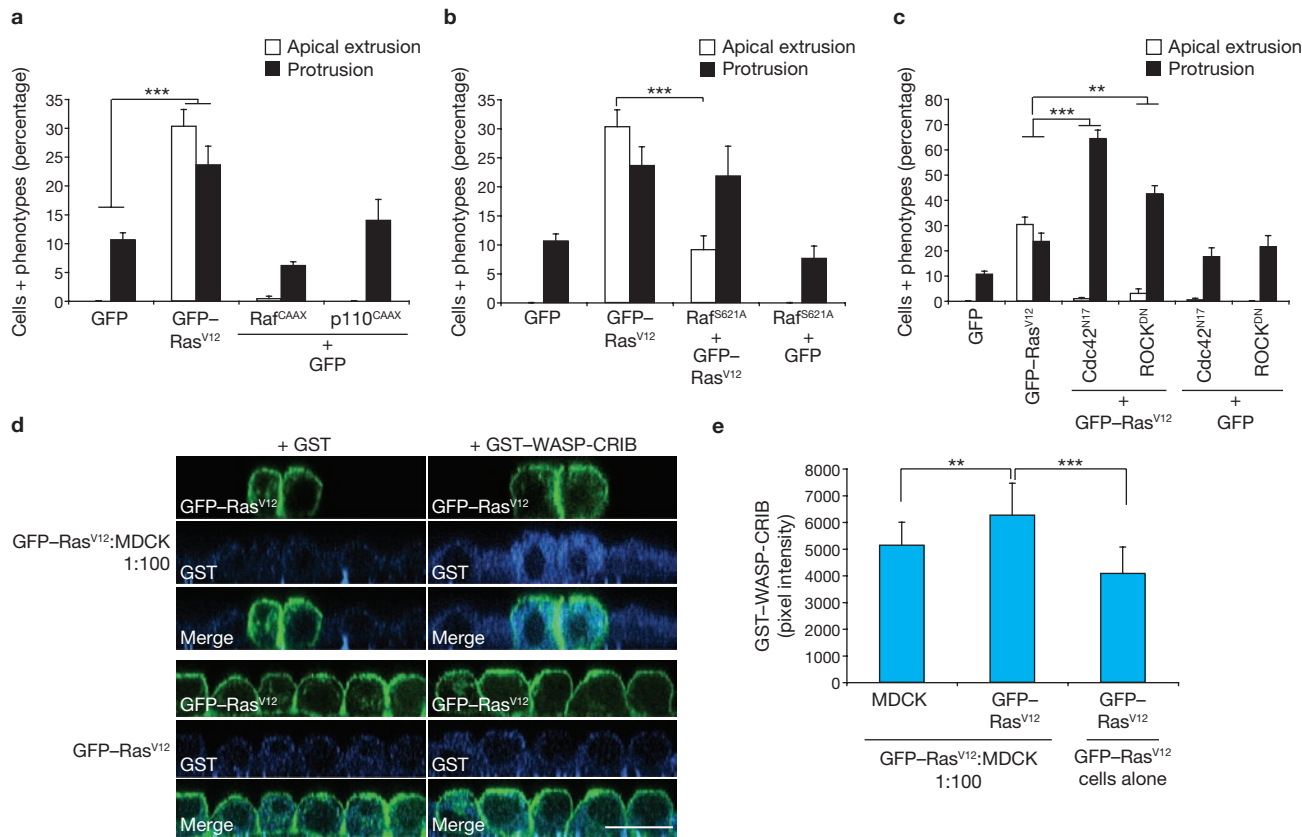


Figure 4. Molecular mechanisms for apical extrusion and basal protrusion formation of Ras^{V12} cells in a monolayer of normal cells. (a, b) Involvement of MAPK and PI(3)K pathways. Indicated proteins were transiently expressed in MDCK cells, and transfected cells that were apically extruded or formed basal protrusions were quantified. GFP or GFP-Ras^{V12} was expressed with or without dominant-active Raf (Raf^{CAAX}) or PI(3)K (p110^{CAAX}, a). GFP or GFP-Ras^{V12} was expressed with or without dominant-negative Raf (Raf^{S621A}, b). For each experiment 50–150 cells were counted; ***P < 0.0001. (c) Involvement of Cdc42 and ROCK. GFP or GFP-Ras^{V12} was expressed with or without constitutively inactive Cdc42 (Cdc42^{N17}) or dominant-negative ROCK (ROCK^{DN}) in MDCK cells, and the transfected cells that were apically extruded or formed basal protrusions were quantified. For

each experiment 50–115 cells were counted; **P < 0.005 ***P < 0.0001. White bar, cells that are apically extruded; black bar, cells that form major protrusions (a–c). (d, e) Non-cell-autonomous activation of Cdc42 in Ras^{V12} cells. Confocal images of MDCK-pTR GFP-Ras^{V12} cells (d) in a monolayer of normal MDCK cells (upper panels) or MDCK-pTR GFP-Ras^{V12} cells (lower panels). Eight hours after tetracycline addition, cells were fixed and incubated with GST (left panels) or GST-WASP-CRIB proteins (right panels), followed by immunostaining with anti-GST antibody (cyan) and Hoechst (blue). Scale bar, 20 µm. WASP-CRIB staining was quantified (e). Data are mean ± s.e.m.; **P < 0.005 ***P < 0.0001; n = 55, 50 and 65 cells for each condition, respectively. Data are mean ± s.e.m. from more than five independent experiments in a, b and c.

adherens junctions are specifically disrupted at the interface between Ras^{V12} and normal cells where protrusions are formed (Supplementary Discussion and Supplementary Information, Fig. S5). Ras^{V12} cells also formed major protrusions when cultured with normal cells on a collagen matrix (Fig. 3f, white arrows and arrowhead). Such protrusions extended beneath neighbouring normal cells and into the collagen. When cells were cultured for longer periods (120 h), non-extruded Ras^{V12} cells invaded the collagen and proliferated underneath the normal cells (Fig. 3g). This occurred non-cell-autonomously, as in a monolayer of only Ras^{V12} cells, Ras^{V12} cells did not form major protrusions nor invade the collagen (0%, n = 25 independent experiments; Fig. 1c, lower right panels). Basal extrusion of Ras^{V12} cells was also observed *in vivo* in the wing imaginal disc epithelium of *Drosophila* (40%, n = 85; Supplementary Information, Fig. S3c).

The molecular mechanisms of apical extrusion and basal protrusion formation of Ras^{V12} cells were further studied using transient expression systems. First, we confirmed that transient transfection of MDCK cells with GFP-Ras^{V12} induced apical extrusion and basal protrusions comparable

to those observed in MDCK-pTR GFP-Ras^{V12} cells (Fig. 4a). Expression of dominant-active Raf (Raf^{CAAX}) alone induced neither apical extrusion nor basal protrusions (Fig. 4a; Supplementary Information, Fig. S6a). Co-expression of dominant-negative Raf markedly suppressed Ras^{V12}-induced MAPK activation and apical extrusion (Fig. 4b; Supplementary Information, Fig. S6a). These results suggest that the MAPK pathway is required, but not sufficient, to promote apical extrusion of Ras^{V12} cells. Expression of dominant-active PI(3)K (p110^{CAAX}) alone promoted neither apical extrusion nor basal protrusion formation (Fig. 4a), whereas addition of LY294002 significantly suppressed basal protrusion formation (Fig. 3e), suggesting that the PI(3)K pathway is required, but not sufficient, to induce basal protrusions. These results suggest an involvement of other Ras targets in these processes¹⁰.

ROCK induces phosphorylation of myosin light chain and activates myosin-II (Supplementary Information, Fig. S7a)¹¹. Co-expression of dominant-negative ROCK (ROCK^{DN}) significantly inhibited Ras^{V12}-induced phosphorylation of myosin light chain (Supplementary Information, Fig. S7b, c). It also decreased apical extrusion while

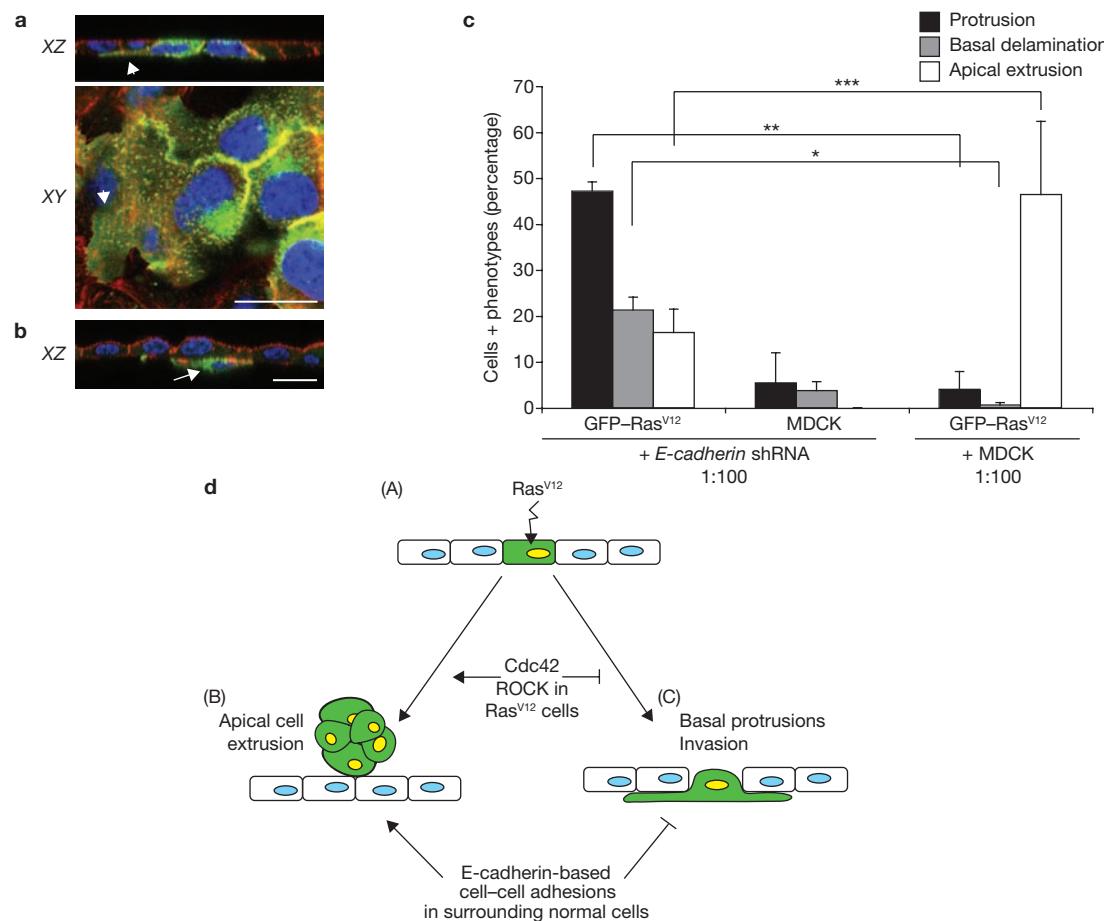


Figure 5. E-cadherin-based intercellular adhesions of surrounding normal cells can influence the fate of Ras^{V12} cells. **(a, b)** Confocal images of MDCK pTR-Ras^{V12} cells combined with MDCK cells expressing E-cadherin shRNA, on collagen gels. After 24 h of tetracycline addition, cells were stained with TRITC-phalloidin (red) and Hoechst (blue). Arrowheads and arrow indicate the basal protrusions and a basally delaminated Ras^{V12} cell, respectively. Scale bars represent 20 μ m. **(c)** Quantification of basal protrusion formation (black bar), basal delamination (grey bar) or apical extrusion (white bar) of GFP-Ras^{V12} or MDCK cells surrounded by E-cadherin shRNA expressing MDCK ($n = 301$ and 396, respectively) or normal MDCK ($n = 536$) cells. Values represent

mean \pm s.d.; * $P < 0.05$ ** $P < 0.005$ *** $P < 0.0005$; n , cells. **(d)** Model showing that (A) when expression of Ras^{V12} is induced in a single epithelial cell (green) within a monolayer of normal cells, two independent phenomena can occur in a non-cell-autonomous fashion. Ras^{V12}-expressing cells are either (B) apically extruded from the monolayer or (C) form basal protrusions beneath the surrounding neighbours. After apical extrusion, Ras^{V12} cells are viable and form multicellular aggregates above the monolayer of normal cells. Ras^{V12} cells that form basal protrusions frequently invade collagen. The fate of Ras^{V12} cells is influenced by the activity of Cdc42 and ROCK in Ras^{V12} cells and by E-cadherin-based cell–cell adhesions in the surrounding normal cells.

increasing basal protrusion formation (Fig. 4c), suggesting an important role of ROCK in these processes. We also examined whether Rho GTPases, crucial regulators for cytoskeletons and cell morphology^{12,13}, have a role in these processes. Co-expression of constitutively inactive Cdc42 (Cdc42^{N17}) with Ras^{V12} strongly suppressed apical extrusion and enhanced basal protrusion formation (Fig. 4c), whereas co-expression of constitutively inactive Rac had no effect on these processes (Supplementary Information, Fig. S7d), indicating that Cdc42 is another crucial regulator in these phenomena. Expression of Cdc42^{N17} or ROCK^{DN} significantly suppressed the effect of Ras^{V12} on cell height and intercellular F-actin accumulation (Supplementary Information, Fig. S7e, f). However, the effect of ROCK^{DN} on cell height was much weaker than that of Cdc42^{N17}, and vice versa, on F-actin accumulation, suggesting that the effects of these two proteins are mediated, at least partially, by different downstream pathways. Using a recombinant protein for the Cdc42-binding domain (CRIB) of WASP (Supplementary Information, Fig. S6b), we found that the amount of GTP-bound active

Cdc42 was substantially increased in Ras^{V12} cells surrounded by normal cells (Fig. 4d and e). In contrast, it was significantly reduced in Ras^{V12} cells surrounded by Ras^{V12} cells (Fig. 4d, e)¹⁴. Taken together, these results indicate that Cdc42 is activated in a non-cell-autonomous manner in Ras^{V12} cells surrounded by normal cells, which profoundly influences the fate of Ras^{V12} cells.

Finally, we induced expression of E-cadherin shRNA in the surrounding normal cells, and examined the effect of knockdown of E-cadherin protein on the fate of Ras^{V12} cells. When surrounded by E-cadherin-deficient cells, Ras^{V12} cells produced large basal protrusions more frequently (Fig. 5a, c) and were more often basally delaminated from the monolayer (Fig. 5b, c) than when surrounded by normal cells (Fig. 5c). In contrast, apical extrusion of Ras^{V12} cells was greatly reduced when they were surrounded by E-cadherin-deficient cells (Fig. 5c). No significant basal delamination or protrusion formation was observed when normal cells were surrounded by E-cadherin-deficient cells (Fig. 5c). These results suggest that the fate of Ras^{V12} cells can be influenced by

E-cadherin-based intercellular adhesions of surrounding normal cells. It is possible that basal invasion by Ras-transformed cells may be promoted under pathological conditions where E-cadherin-based cell–cell contacts are not properly formed in the surrounding epithelium, such as chronic inflammation or infection (see Supplementary Information Discussion on the molecular mechanisms of these processes and Fig. S8 for phenomena induced by other oncogenic stimuli).

In *Drosophila*, it has been reported that the interaction between normal and transformed epithelial cells can cause several cellular processes, such as cell extrusion and apoptosis, that occur in a non-cell-autonomous fashion^{15–18}. However, the molecular mechanism whereby normal and transformed cells recognize differences between each other is not clearly understood. Our data also suggest that Ras^{V12} cells recognize that they are surrounded by normal cells. There are two possible molecular mechanisms of cell recognition: cells detect differences either in physical properties of other cells or in the composition of molecules (for example, lipids and proteins) in plasma membranes. We have found that Ras^{V12} cells have higher membrane elasticity and cell viscosity than normal cells (Supplementary discussion and Supplementary Information, Fig. S9). It remains to be determined whether these physical properties are important in initial cell recognition machineries and/or whether there are unidentified molecules that are involved in cell-recognition between normal and transformed cells.

In summary, when Ras^{V12} is expressed in single cells in an epithelial monolayer, two independent phenomena can occur in a non-cell-autonomous manner (Fig. 5d). Ras^{V12}-expressing cells are either apically extruded from the monolayer, or form basal protrusions leading to basal invasion into the matrix. The fate of Ras^{V12} cells is influenced by the activity of Cdc42 and ROCK in Ras^{V12} cells and by E-cadherin-based cell–cell adhesions in the surrounding normal cells. Thus, Ras^{V12} cells leave epithelial sheets either apically or basally in a cell-context-dependent manner. Our data and previous reports suggest that several cellular processes can occur at the interface between normal and transformed cells in *Drosophila* and vertebrates^{15–21}. In future studies, it needs to be further clarified whether these processes indeed occur at the initial step of human carcinogenesis. These investigations may lead to a new preventive or therapeutic treatment for cancer. □

METHODS

Antibodies and materials. Rat anti-E-cadherin (ECCD2) and rabbit anti-ZO-1 antibodies were from Zymed. Mouse anti-β-catenin, mouse anti-E-cadherin and mouse anti-phospho-tyrosine antibodies were from BD Biosciences. Rat and mouse anti-E-cadherin antibodies were used for immunofluorescence and western blotting, respectively. Rat anti-α-tubulin and mouse anti-GFP antibodies were from Abcam and Roche Diagnostics, respectively. Rabbit anti-phosphomyosin light chain 2 (p-MLC; Thr 18/Ser 19) antibody was from Cell Signaling Technology, mouse anti-Pan-Ras antibody was from Calbiochem, Anti-GAPDH antibody was from Chemicon International and mouse anti-gp135 antibody was provided by G. K. Ojakian (SUNY Downstate Medical Center, NY) and used as an apical membrane marker. Mouse anti-β-galactosidase antibody was from Promega. Mouse anti-phospho-MAPK and rabbit anti-GST antibodies were from Sigma-Aldrich and Santa Cruz, respectively. Alexa-568- and Alexa-647-conjugated anti-rat, anti-mouse and anti-rabbit antibodies were from Invitrogen. All primary antibodies were used at a dilution of 1:100 for immunofluorescence, except anti-p-MLC antibody, which was used at 1:25, and anti-phospho-MAPK antibody, which was used at 1:50. All secondary antibodies were used at 1:200. TRITC-phalloidin (Sigma-Aldrich) was used at 1.5 µg ml⁻¹. Hoechst (Invitrogen) was used at 1:5,000. For western blotting, antibodies were used as follows: anti-Pan-Ras at 1:1,000, anti-GFP and anti-E-cadherin at 1:2,000 and anti-GAPDH at 1:5,000.

The following inhibitors were used: 4-AP (2 mM, Sigma-Aldrich), Ethidium homodimer-1 (Ethd-1, 1 µM, Invitrogen), (S)-(–)-blebbistatin (50 µM, Toronto Research Chemicals), U0126 (10 µM, Promega), LY294002 and Y27632 (10 µM, Calbiochem) and cytochalasin D (100 nM, Sigma-Aldrich). All inhibitors were added at the beginning of the experiments for 16–24 h incubation. DMSO (Sigma-Aldrich) was added at a dilution of 1:1,000 as a control.

Time-lapse microscopy. MDCK cells stably expressing GFP-Ras^{V12} or GFP-Rap1^{V12} were fluorescently labelled using CellTracker dye CMPTX (Invitrogen) according to the manufacturer's instructions. Labelled cells were then trypsinized and combined with MDCK cells at a ratio of 1:100. Cells were plated at a density of 1 × 10⁶ cells per well in 35 mm glass-bottom culture dishes (MatTek Corporation) for all experiments. Mixed cells were incubated for 8 h at 37 °C before being transferred to a tetracycline-containing medium. Where indicated, cells were analysed in the presence of 4-AP. To obtain time-lapse images, we used a Zeiss Axiovert 200 M microscope with a Ludd Electronic Products Biopoint Controller and a Hamamatsu C4742-95 Orca camera (Hamamatsu). Images were captured and analysed using Openlab or Volocity software (Improvision).

Collagen assays. Type-I collagen was obtained from R&D Systems (Cultrex Rat Collagen I) or Nitta Gelatin (Nitta Cellmatrix type 1-A), and was neutralized on ice to a final concentration of 2 mg ml⁻¹ according to the manufacturer's instructions. Glass coverslips in 6-well culture dishes were coated with 1 ml of neutralized collagen and allowed to solidify for 30 min at 37 °C. For time-lapse experiments, 35 mm glass-bottom dishes were pre-coated with a thin layer (approximately 200 µl) of neutralized collagen. For each assay, between 5 × 10⁵ and 1 × 10⁶ cells were plated per well onto the collagen gel. Ras^{V12} cells were combined with MDCK cells at a ratio of 1:100. After incubation for 8–16 h at 37 °C, tetracycline was added to induce Ras^{V12} expression. A control (absence of tetracycline) was also included for each experiment. Cells were incubated for the indicated times, and tetracycline was replaced every 48 h.

For immunostaining, cells on collagen were fixed with 4% paraformaldehyde/PBS for 15 min at 37 °C, washed three times in PBS and permeabilized in 0.5% Triton X-100/PBS for 20 min. Cells were then washed once in PBS followed by three 10-min washes in glycine wash buffer (7 mM Na₂HPO₄, 3.5 mM NaH₂PO₄, 130 mM NaCl and 100 mM glycine). Cells were blocked for 1 h in blocking buffer (7 mM Na₂HPO₄, 3.5 mM NaH₂PO₄, 130 mM NaCl, 0.2% Triton X-100, 0.05% Tween-20, 10% FCS, 0.02% BSA and 7.7 mM Na₃N), and incubated with primary antibodies for 16 h at 4 °C. This was followed by three 10-min washes with gentle agitation in blocking buffer before incubation with Alexa-568- and Alexa-647-conjugated secondary antibodies and/or TRITC-phalloidin for 2–3 h at room temperature. Cells were then washed three times in blocking buffer and were incubated with Hoechst/PBS for 2 min, followed by washing in PBS and mounting onto Mowiol on a glass slide.

Cdc42 activation assay. The level of active GTP-bound Cdc42 in cells was determined using a GST fusion protein containing the Cdc42-interacting domain of WASP (WASP-CRIB)²². GST or GST-WASP-CRIB protein was produced as described previously^{22,23}. After fixation, permeabilization and blocking as described above, cells were incubated with 100 ng ml⁻¹ of GST or GST-WASP-CRIB protein in blocking buffer for 1 h at room temperature, followed by three 10-min washes with gentle agitation in blocking buffer before incubation with anti-GST antibody for 16 h at 4 °C. After three 10-min washes with gentle agitation in blocking buffer, cells were incubated with Alexa-647-conjugated secondary antibody for 2 h at room temperature. Cells were then washed three times in blocking buffer, incubated with Hoechst/PBS for 2 min and mounted onto Mowiol on a glass slide.

Generation and analyses of Ras overexpressing clones in *Drosophila* wing imaginal discs. Experimental genotypes were: Ras^{V12}: hs-FLP/+; tub>>Gal4 UAS-lacZ/UAS-ras^{V12}; Ras^{WT}: hs-FLP/UAS-ras^{WT}; tub>>Gal4 UAS-lacZ/+; Ras^{WT}: hs-FLP/+; tub>>Gal4 UAS-lacZ/UAS-ras^{WT}. Clones were induced by heat-shocking larvae three days after egg laying (AEL) for 30 min at 37 °C. Larvae were dissected 68–72 h after clone induction and fixed in 4% paraformaldehyde/PBS. Dissected hemilarvae were permeabilized in 0.05% TritonX-100/PBS (PBT) and incubated for 30 min in 4% FCS/PBT. Samples were incubated with a primary antibody (mouse anti β-galactosidase) for 16 h at 4 °C, and then with Alexa-488-conjugated secondary antibody in 4% FCS/PBT for 2 h at room temperature. After

each incubation with an antibody, samples were extensively washed in PBT. Nuclei were counterstained with Hoechst/PBS for 15 min at room temperature. Imaging was performed on a confocal Leica SPE acquiring xz sections every 0.75–1.0 μm . To induce the expression of Ras^{V12} in the entire wing disc, we drove the expression of UAS-Ras^{V12} under the control of *nubbin*-Gal4 at 25 °C.

Data analyses. All statistical analyses were carried out using Student's *t* tests. Detailed statistical analyses are described in Supplementary Information Methods.

Note: Supplementary Information is available on the Nature Cell Biology website.

ACKNOWLEDGEMENTS

We thank G. K. Ojakian for the anti-gp135 antibody, A. Hall, A. Lloyd, R. Y. Tsien, S. Lowe and E. Sahai for constructs, and A. Vaughan for technical assistance with microscopes. We also thank Y. Morishita for discussion on physical forces at cell-cell adhesions. S.D.-C. was supported by a FEBS Long Term Fellowship. A.E.P. acknowledges the Interdisciplinary Research Collaboration (IRC) in Nanotechnology (Cambridge, EPSRC UK) and the Dr Mortimer and Theresa Sackler Trust for financial support. This work is supported by MRC funding of the Cell Biology Unit.

AUTHOR CONTRIBUTIONS

C.H. designed the experiments and generated most of the data; S.D.-C. established stable MDCK cell lines and performed statistical analyses (Fig. 1d); M.N. analysed clonal expression of Ras^{V12}, Ras^{N17} and Ras^{WT} in *Drosophila* wing imaginal discs (Fig. 1e and Supplementary Information, Fig. S3); M.K. performed western blot analyses (Supplementary Information, Fig. S1b), immunofluorescence studies (Supplementary Information, Fig. S4a) and established stable MDCK cell lines; C.Z. performed western blot and time-lapse analyses (Supplementary Information, Figs S2a, d and S5e), and established stable MDCK cell lines; A.E.P. performed AFM experiments and analyses (Supplementary Information, Fig. S9); E.P., L.A.B.-L. and J.-P.V. analysed clonal expression of Ras^{V12}, Ras^{N17} and Ras^{WT} in *Drosophila* wing imaginal discs (Fig. 1e and Supplementary Information, Fig. S3); Y.I. provided technical expertise on use of collagen; H.H. provided technical expertise on myosin-II; F.P. assisted with *Drosophila* experiments; Y.F. conceived and designed the study and acted as principal investigator.

COMPETING FINANCIAL INTERESTS

The authors declare no competing financial interests.

Published online at <http://www.nature.com/naturecellbiology/>

Reprints and permissions information is available online at <http://npg.nature.com/reprintsandpermissions/>

1. Hanahan, D. & Weinberg, R. A. The hallmarks of cancer. *Cell* 100, 57–70 (2000).
2. Fialkow, P. J. Clonal origin of human tumors. *Biochim. Biophys. Acta* 458, 283–321 (1976).

3. Nowell, P. C. The clonal evolution of tumor cell populations. *Science* 194, 23–28 (1976).
4. Schoenenberger, C. A., Zuk, A., Kendall, D. & Matlin, K. S. Multilayering and loss of apical polarity in MDCK cells transformed with viral K-ras. *J. Cell Biol.* 112, 873–889 (1991).
5. Rosenblatt, J., Raff, M. C. & Cramer, L. P. An epithelial cell destined for apoptosis signals its neighbors to extrude it by an actin- and myosin-dependent mechanism. *Curr. Biol.* 11, 1847–1857 (2001).
6. Bos, J. L. Ras-like GTPases. *Biochim. Biophys. Acta* 1333, M19–31 (1997).
7. Baena-Lopez, L. A., Pastor-Pareja, J. C. & Resino, J. Wg and Egfr signalling antagonise the development of the peripodial epithelium in *Drosophila* wing discs. *Development* 130, 6497–6506 (2003).
8. Rodriguez-Viciana, P. *et al.* Role of phosphoinositide 3-OH kinase in cell transformation and control of the actin cytoskeleton by Ras. *Cell* 89, 457–467 (1997).
9. Cantrell, D. A. Phosphoinositide 3-kinase signalling pathways. *J. Cell Sci.* 114, 1439–1445 (2001).
10. Karnoub, A. E. & Weinberg, R. A. Ras oncogenes: split personalities. *Nature Rev. Mol. Cell Biol.* 9, 517–531 (2008).
11. Kimura, K. *et al.* Regulation of myosin phosphatase by Rho and Rho-associated kinase (Rho-kinase). *Science* 273, 245–248 (1996).
12. Jaffe, A. B. & Hall, A. Rho GTPases: biochemistry and biology. *Annu. Rev. Cell Dev. Biol.* 21, 247–269 (2005).
13. Vega, F. M. & Ridley, A. J. Rho GTPases in cancer cell biology. *FEBS Lett.* 582, 2093–2101 (2008).
14. Sahai, E., Olson, M. F. & Marshall, C. J. Cross-talk between Ras and Rho signalling pathways in transformation favours proliferation and increased motility. *EMBO J.* 20, 755–766 (2001).
15. de la Cova, C., Abril, M., Bellota, P., Gallant, P. & Johnston, L. A. *Drosophila* Myc regulates organ size by inducing cell competition. *Cell* 117, 107–116 (2004).
16. Moreno, E. & Basler, K. dMyc transforms cells into super-competitors. *Cell* 117, 117–129 (2004).
17. Vidal, M., Larson, D. E. & Cagan, R. L. Csk-deficient boundary cells are eliminated from normal *Drosophila* epithelia by exclusion, migration, and apoptosis. *Dev. Cell* 10, 33–44 (2006).
18. Brumby, A. M. & Richardson, H. E. scribble mutants cooperate with oncogenic Ras or Notch to cause neoplastic overgrowth in *Drosophila*. *EMBO J.* 22, 5769–5779 (2003).
19. Stoker, M. G., Shearer, M. & O'Neill, C. Growth inhibition of polyoma-transformed cells by contact with static normal fibroblasts. *J. Cell Sci.* 1, 297–310 (1966).
20. Bignami, M., Rosa, S., La Rocca, S. A., Falcone, G. & Tato, F. Differential influence of adjacent normal cells on the proliferation of mammalian cells transformed by the viral oncogenes myc, ras and src. *Oncogene* 2, 509–514 (1988).
21. Alexander, D. B. *et al.* Normal cells control the growth of neighboring transformed cells independent of gap junctional communication and SRC activity. *Cancer Res.* 64, 1347–1358 (2004).
22. Wells, C. M., Walmsley, M., Ooi, S., Tybulewicz, V. & Ridley, A. J. Rac1-deficient macrophages exhibit defects in cell spreading and membrane ruffling but not migration. *J. Cell Sci.* 117, 1259–1268 (2004).
23. Hogan, C. *et al.* Rap1 regulates the formation of E-cadherin-based cell-cell contacts. *Mol. Cell. Biol.* 24, 6690–6700 (2004).

DOI: 10.1038/ncb1853

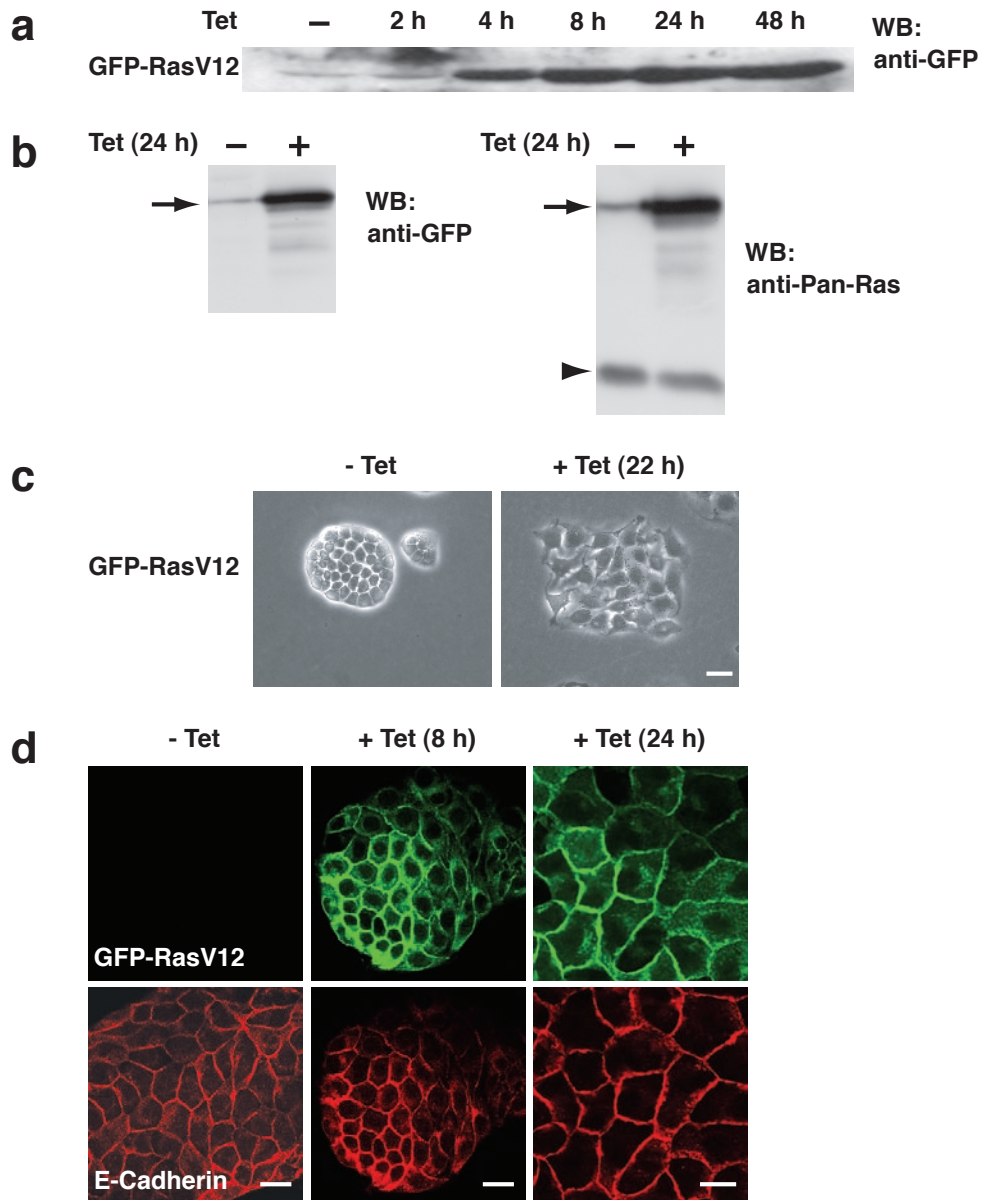


Figure S1 Establishment of a tetracycline-inducible system for GFP-tagged RasV12 in MDCK epithelial cells. **a** Tetracycline-induced expression of GFP-RasV12 protein in MDCK-pTR cells as determined by Western blotting using anti-GFP antibody. **b** Comparison of expression level of exogenous GFP-RasV12 (arrows) and endogenous Ras (arrowhead) proteins. Following 24 h of tetracycline addition, cell lysates of MDCK-pTR GFP-RasV12 cells were

examined by Western blotting with anti-GFP and anti-Pan-Ras antibodies. **c** Phase contrast images of MDCK-pTR GFP-RasV12 cells cultured at low density without tetracycline (left) or with tetracycline (right). Scale bar, 10 μ m. **d** Confocal images of GFP-RasV12 cells cultured at high density and stained with anti-E-cadherin antibody (red) without or with tetracycline induction (8 h or 24 h). Scale bars, 20 μ m.

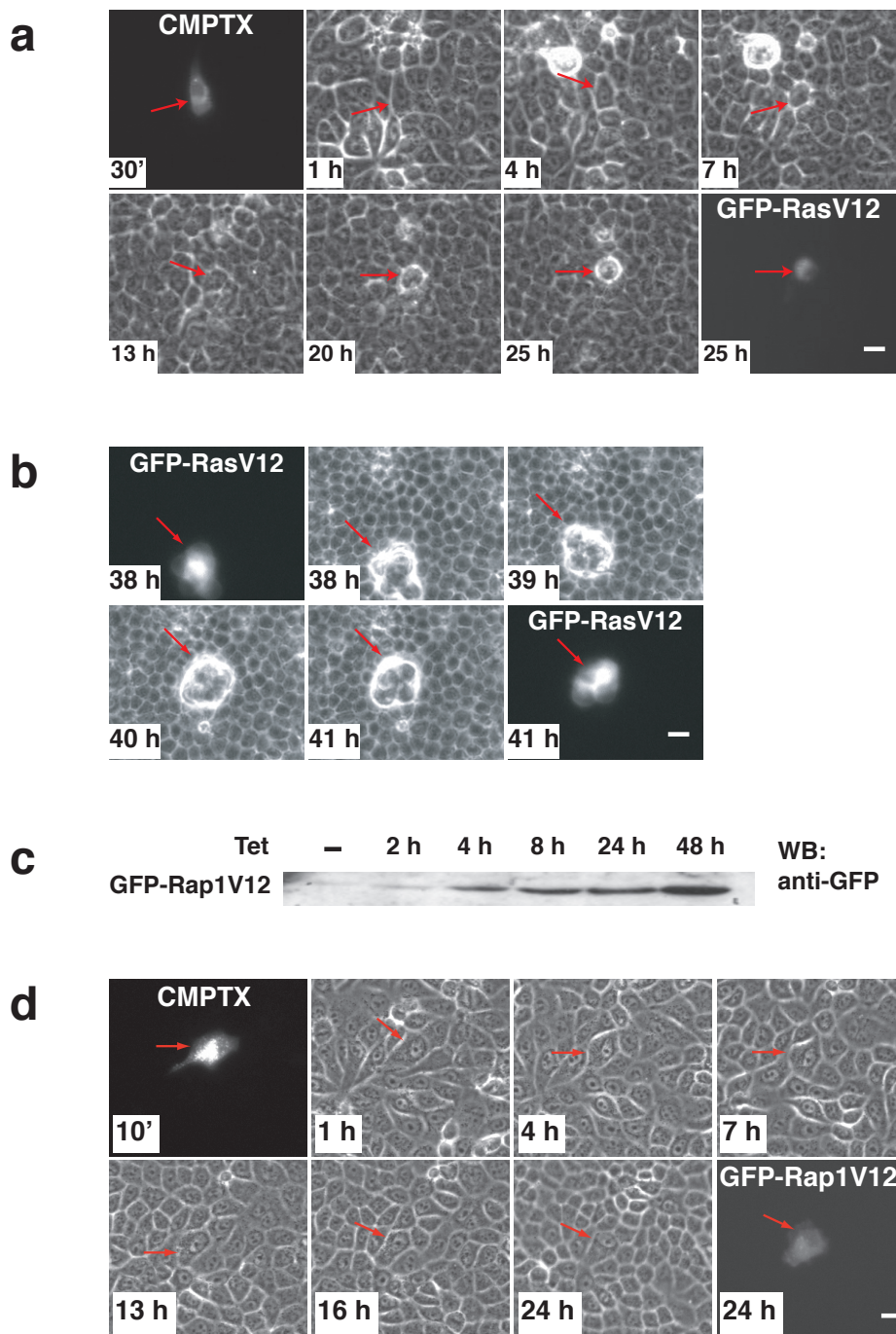


Figure S2 **a** A single RasV12-expressing cell is extruded from a monolayer of non-transformed cells. Fluorescently labelled MDCK-pTR GFP-RasV12 cells (CMPTX) were cultured with non-transformed MDCK cells at a ratio of 1:100 on collagen gels, followed by tetracycline treatment. Red arrows indicate a fluorescently labelled RasV12 cell. **b** Apically extruded RasV12 cells form multicellular aggregates that dynamically move over the apical surface of the non-transformed cells. GFP-RasV12 cells mixed with non-transformed MDCK cells were seeded on collagen. Once a monolayer was formed, RasV12 expression was induced with tetracycline and cells were monitored using time-lapse microscopy. Red arrows indicate a Rap1V12 cell. **a, b, d**; Images are extracted from a representative time-lapse analysis. Scale bars, 20 μ m.

Red arrows indicate RasV12 cells. **c** Tetracycline-induced expression of GFP-Rap1V12 protein in MDCK-pTR cells as determined by Western blotting using anti-GFP antibody. **d** GFP-Rap1V12 cells are not extruded from a monolayer of non-transformed MDCK cells. GFP-Rap1V12 cells were pre-stained with fluorescent dye (CMPTX), and mixed with non-transformed MDCK cells at a ratio of 1:100. Once a monolayer was formed, Rap1V12 expression was induced with tetracycline and cells were monitored using time-lapse microscopy. Red arrows indicate a Rap1V12 cell. **a, b, d**; Images are extracted from a representative time-lapse analysis. Scale bars, 20 μ m.

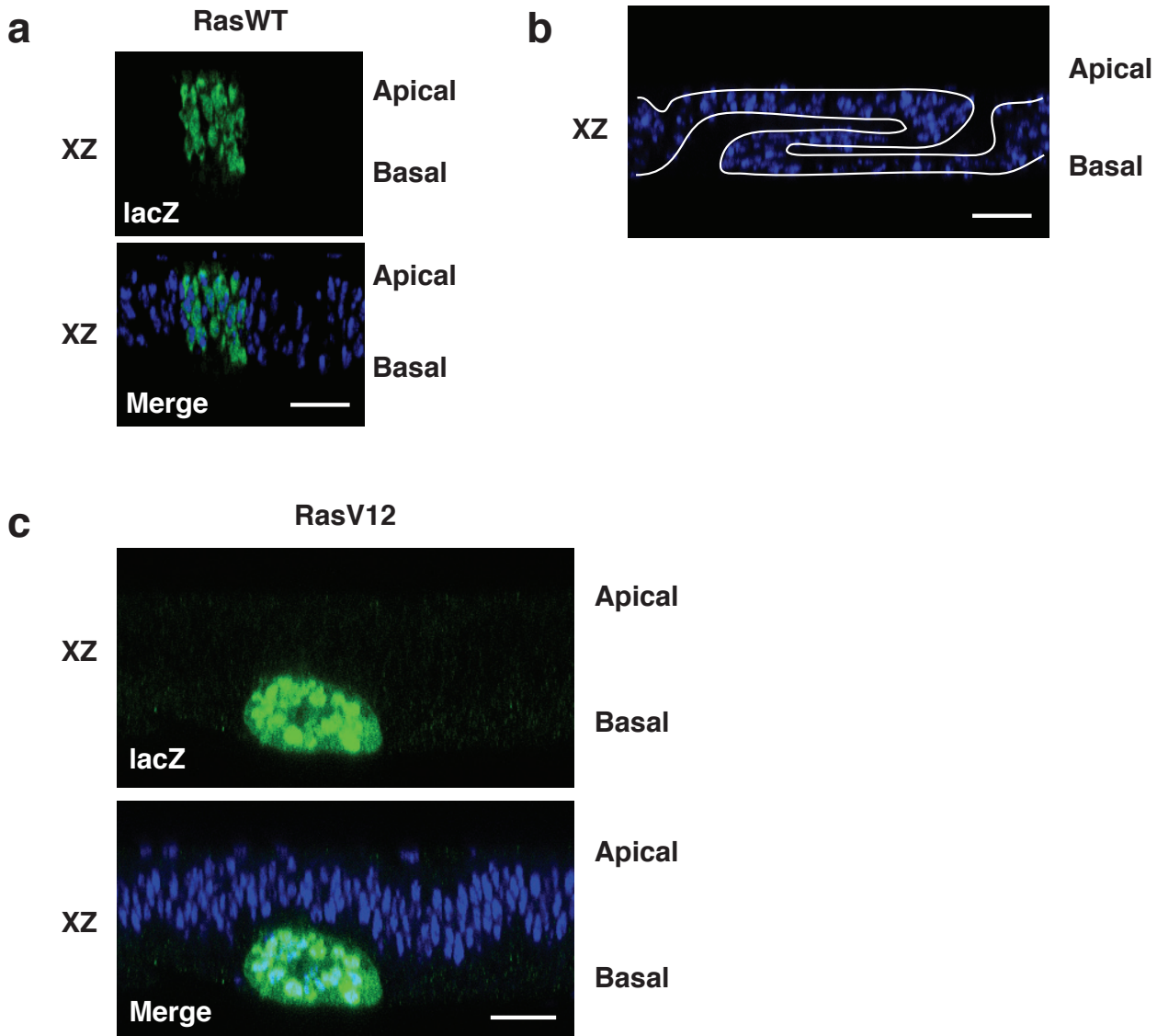


Figure S3 **a** RasWT-expressing cells are not apically extruded from a normal epithelium *in vivo*. Confocal images of *Drosophila* wing imaginal disc epithelium co-expressing lacZ and RasWT in a mosaic manner. Cells were stained with anti- β -galactosidase antibody (green) and Hoechst (blue).

monolayer becomes irregularly folded. Cells were stained with Hoechst (blue). **c** RasV12-expressing cells are basally delaminated from a normal epithelium *in vivo*. Confocal images of *Drosophila* wing imaginal disc epithelium co-expressing lacZ and RasV12 in a mosaic manner. Cells were stained with anti- β -galactosidase antibody (green) and Hoechst (blue). **a-c**; scale bars, 20 μ m.

SUPPLEMENTARY INFORMATION

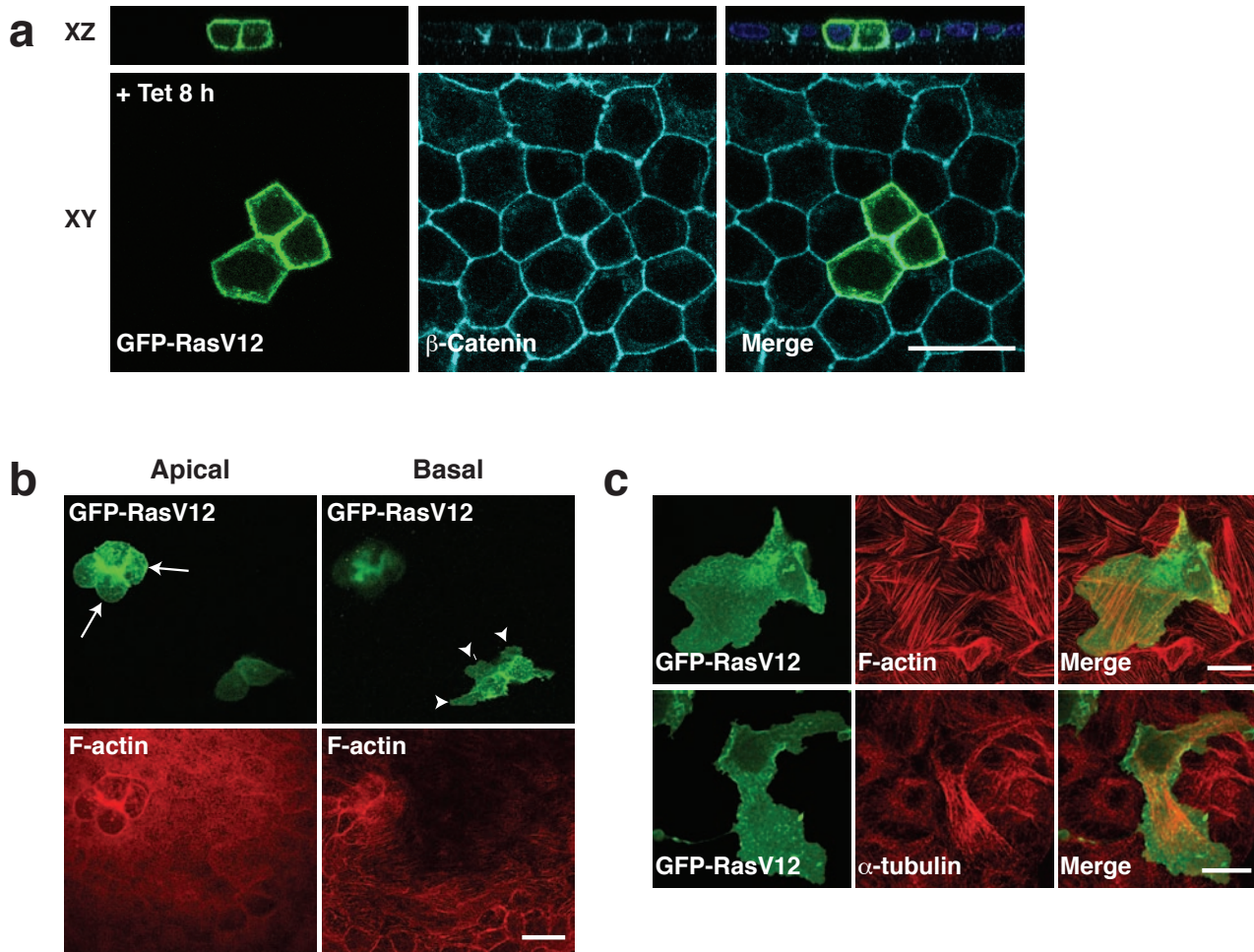


Figure S4 a E-cadherin-based adherens junctions are maintained between GFP-RasV12 cells in a monolayer of normal cells. Confocal images of GFP-RasV12 cells in a monolayer of non-transformed cells. Following 8 h of tetracycline addition, cells were stained with anti- β -catenin antibody (cyan). **b** Apical and basal confocal images of GFP-RasV12 cells in a monolayer of normal MDCK cells on collagen gels. Following 24 h of tetracycline addition,

cells were stained with TRITC-phalloidin (red). White arrows indicate apically extruded RasV12 cells. White arrowheads indicate RasV12 cells that have formed basal protrusions. **c** Confocal images of GFP-RasV12 cells in a monolayer of non-transformed cells. Following 24 h of tetracycline addition, cells were stained with TRITC-phalloidin (top panels) or anti- α -tubulin antibody (bottom panels). **a-c**; scale bars, 20 μ m.

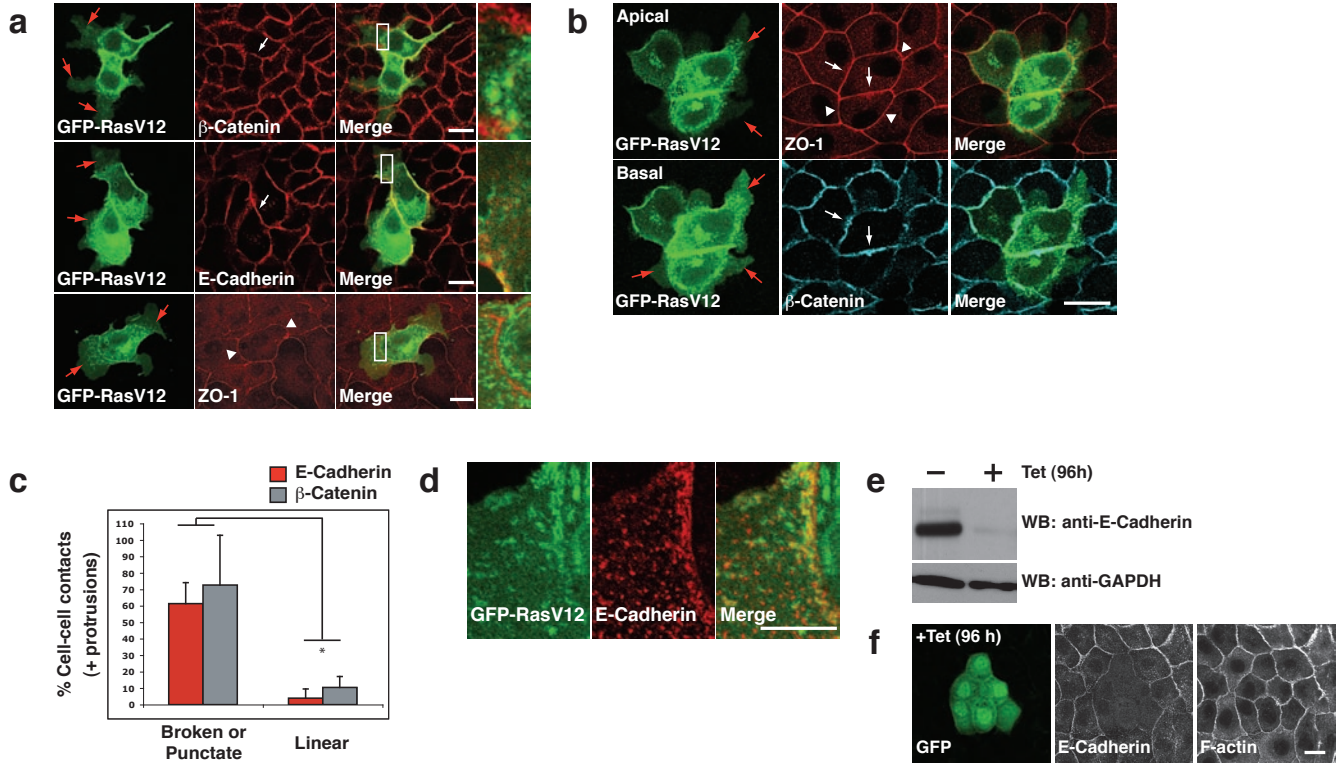


Figure S5 Protrusion formation at the interface between RasV12 and non-transformed cells is associated with disruption of adherens junctions. **a, b** Confocal images of GFP-RasV12 cells mixed with non-transformed cells. Following 8 h incubation with tetracycline, adherens junctions were analysed using anti-E-cadherin and anti- β -catenin antibodies. Tight junctions were analysed using anti-ZO-1 antibody. Red arrows indicate protrusions. White arrows and arrowheads indicate cell-cell contacts between RasV12 cells and those between RasV12 and normal cells where basal protrusions were formed, respectively. The area in the white box of each merge image in **a** is shown in higher magnification on the right. It should be noted that in **b**, cells were double-stained for ZO-1 and β -catenin. **c** Quantification of cell-cell contacts with disrupted (broken or punctate) or linear localisation of E-cadherin (red bar) or β -catenin (grey bar) between normal and RasV12 cells that form protrusions. Values represent mean \pm s.d. *P < 0.05. **d** Confocal images representing magnified view of a protrusion at the interface between GFP-RasV12 and non-transformed cells. Following 8 h incubation with tetracycline, cells were stained with anti-E-cadherin antibody (red). **e** MDCK cells stably expressing E-cadherin shRNA in a tetracycline-inducible manner. Knockdown of E-cadherin protein was detected by Western blotting using anti-E-cadherin antibody, following 96 h of tetracycline addition. Equal protein loading was confirmed using anti-GAPDH antibody. **f** Knockdown of E-cadherin protein does not lead to protrusion formation in a monolayer of normal cells. GFP is constitutively expressed in E-cadherin shRNA cells. F-actin at cell-cell contacts was labelled using TRITC-phalloidin. **a, b, d, f**; scale bars, 20 μ m.

bar) or β -catenin (grey bar) between normal and RasV12 cells that form protrusions. Values represent mean \pm s.d. *P < 0.05. **d** Confocal images representing magnified view of a protrusion at the interface between GFP-RasV12 and non-transformed cells. Following 8 h incubation with tetracycline, cells were stained with anti-E-cadherin antibody (red). **e** MDCK cells stably expressing E-cadherin shRNA in a tetracycline-inducible manner. Knockdown of E-cadherin protein was detected by Western blotting using anti-E-cadherin antibody, following 96 h of tetracycline addition. Equal protein loading was confirmed using anti-GAPDH antibody. **f** Knockdown of E-cadherin protein does not lead to protrusion formation in a monolayer of normal cells. GFP is constitutively expressed in E-cadherin shRNA cells. F-actin at cell-cell contacts was labelled using TRITC-phalloidin. **a, b, d, f**; scale bars, 20 μ m.

SUPPLEMENTARY INFORMATION

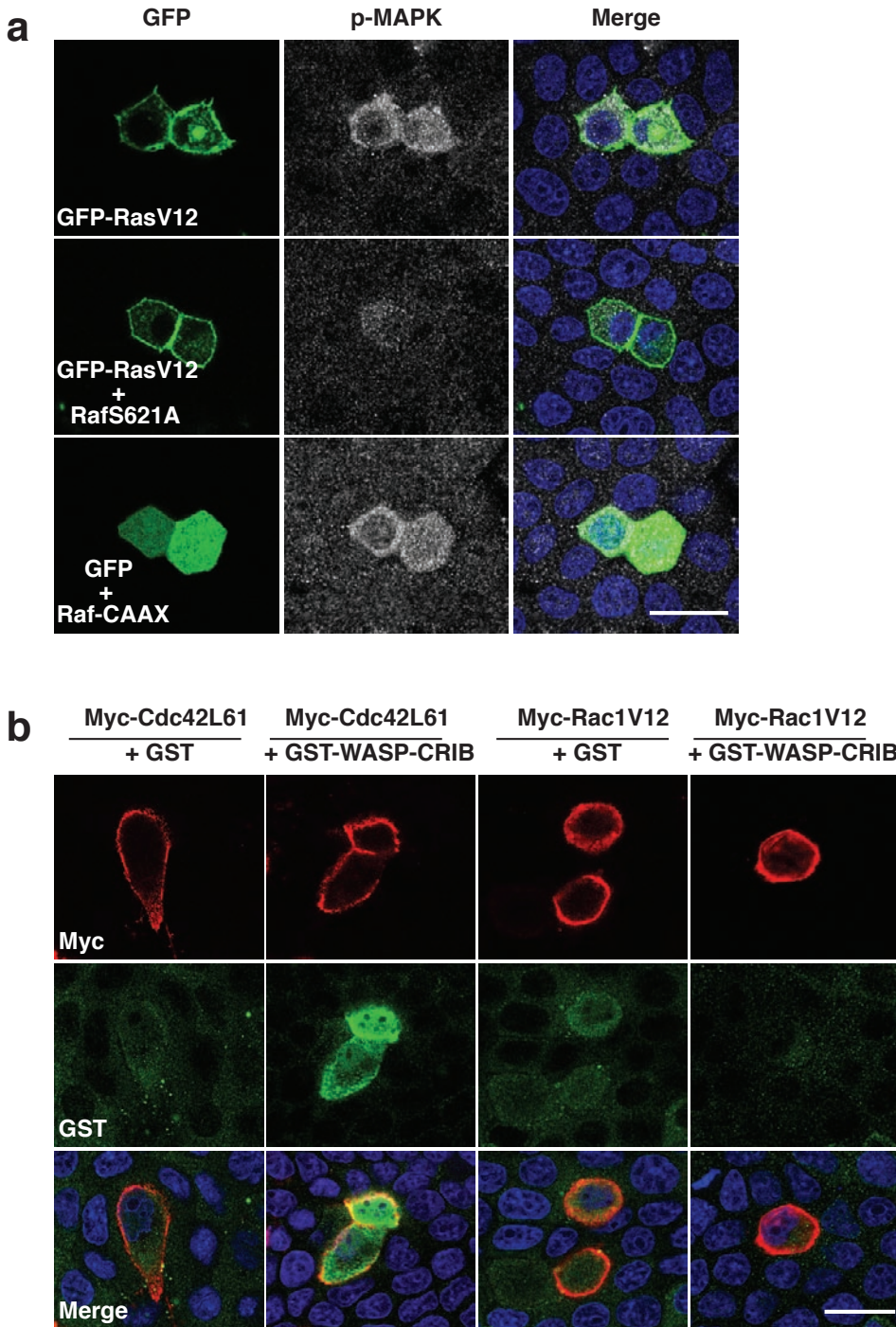


Figure S6 a Confocal images of MDCK cells transiently expressing GFP-RasV12 (top), GFP-RasV12 and dominant negative Raf (RafS621A) (middle), or GFP and dominant active Raf (Raf-CAAX) (bottom). Active MAPK was detected using anti-phospho-MAPK antibody (grey), and nuclei were stained with Hoechst (blue).

b The Cdc42-binding domain (CRIB domain) of WASP protein specifically binds to GTP-bound Cdc42 but not to GTP-bound Rac1. Confocal images of MDCK cells transiently expressing constitutively active Cdc42 (Myc-Cdc42L61) or Rac1 (Myc-Rac1V12). Fixed cells were incubated with GST or GST-WASP-CRIB protein, followed by immunostaining with anti-GST (green), anti-myc (red) antibodies and Hoechst (blue). **a, b;** scale bar, 20 μ m.

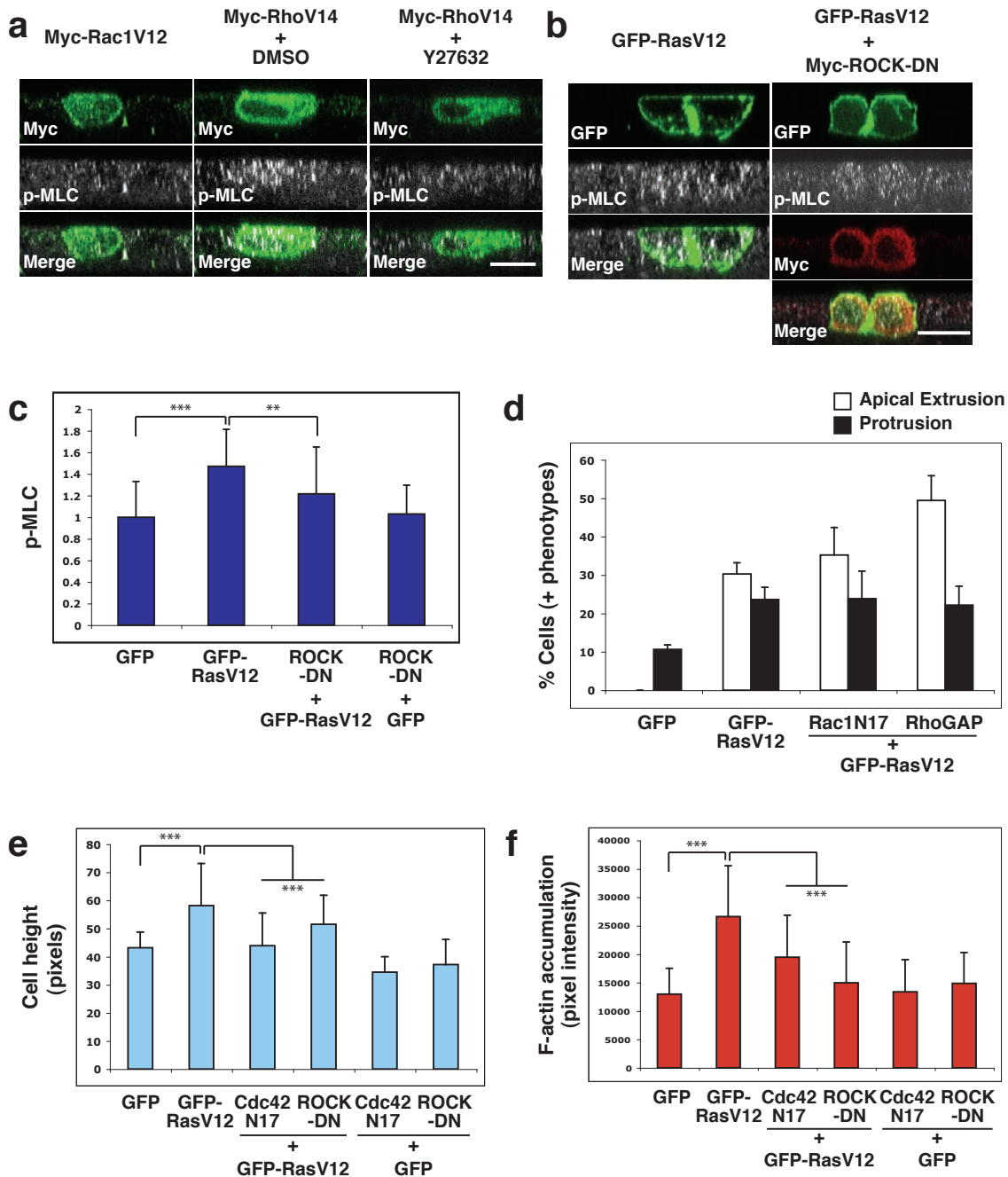


Figure S7 Molecular mechanisms for apical extrusion and basal protrusion formation of RasV12 cells using a transient expression system. **a** Confocal images of MDCK cells transiently expressing constitutively active Rac1 (Myc-Rac1V12) or RhoA (Myc-RhoV14). RhoA-expressing cells were incubated with or without ROCK inhibitor Y27632. Fixed cells were stained with anti-myc (green) and phospho-MLC (grey) antibodies. These results suggest specific immunostaining of phospho-MLC. **b** Confocal images of MDCK cells transiently expressing GFP-RasV12 with or without dominant negative ROCK (Myc-ROCK-DN). Fixed cells were stained with anti-myc (red) and phospho-MLC (grey) antibodies. **c** Quantification of immunofluorescence of phosphorylated myosin light chain (p-MLC) in MDCK cells that transiently express GFP or

GFP-RasV12 with or without dominant negative ROCK (ROCK-DN). Values are expressed as a ratio relative to those in GFP-transfected cells, and represent mean \pm s.e.m. *** $P < 0.0001$ ** $P < 0.005$. **d** Quantification of apical extrusion (white bar) and basal protrusion formation (black bar) of MDCK cells that transiently express GFP- or GFP-RasV12 with or without constitutively inactive Rac1 (Rac1N17) or RhoGAP. Values represent mean \pm s.e.m. It should be noted that expression of constitutively inactive RhoN19 was toxic for MDCK cells and could not be used for analyses. **e, f** Quantification of **e** cell height or **f** intercellular F-actin of MDCK cells that transiently express GFP or GFP-RasV12 with or without constitutively inactive Cdc42 (Cdc42N17) or ROCK-DN. Values represent mean \pm s.d. *** $P < 0.0001$. **a, b**; Scale bars, 20 μ m.

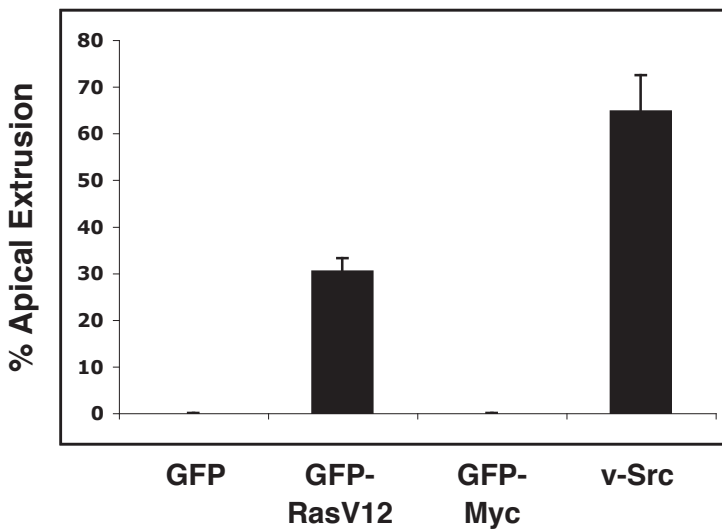


Figure S8 Quantification of apical extrusion of MDCK cells that transiently express GFP-, GFP-RasV12, GFP-Myc or v-Src. Values represent mean \pm s.e.m. Expression of v-Src was monitored by immunofluorescence using anti-phospho-tyrosine antibody. For each construct, more than 50 cells from 2-5 independent experiments were analysed. pmCherry or pEGFP was cotransfected with pCDNA/TO/GFP-Myc or pSG-v-Src to analyse the

formation of basal protrusions. It should be noted that basal protrusion formation was not substantially observed in MDCK cells expressing GFP-Myc or v-Src under these experimental conditions (data not shown). We also found that MDCK cells transiently transfected with pRK5-myc RasV12 and pEGFP formed basal protrusions comparable to those observed in cells expressing GFP-RasV12 (data not shown).

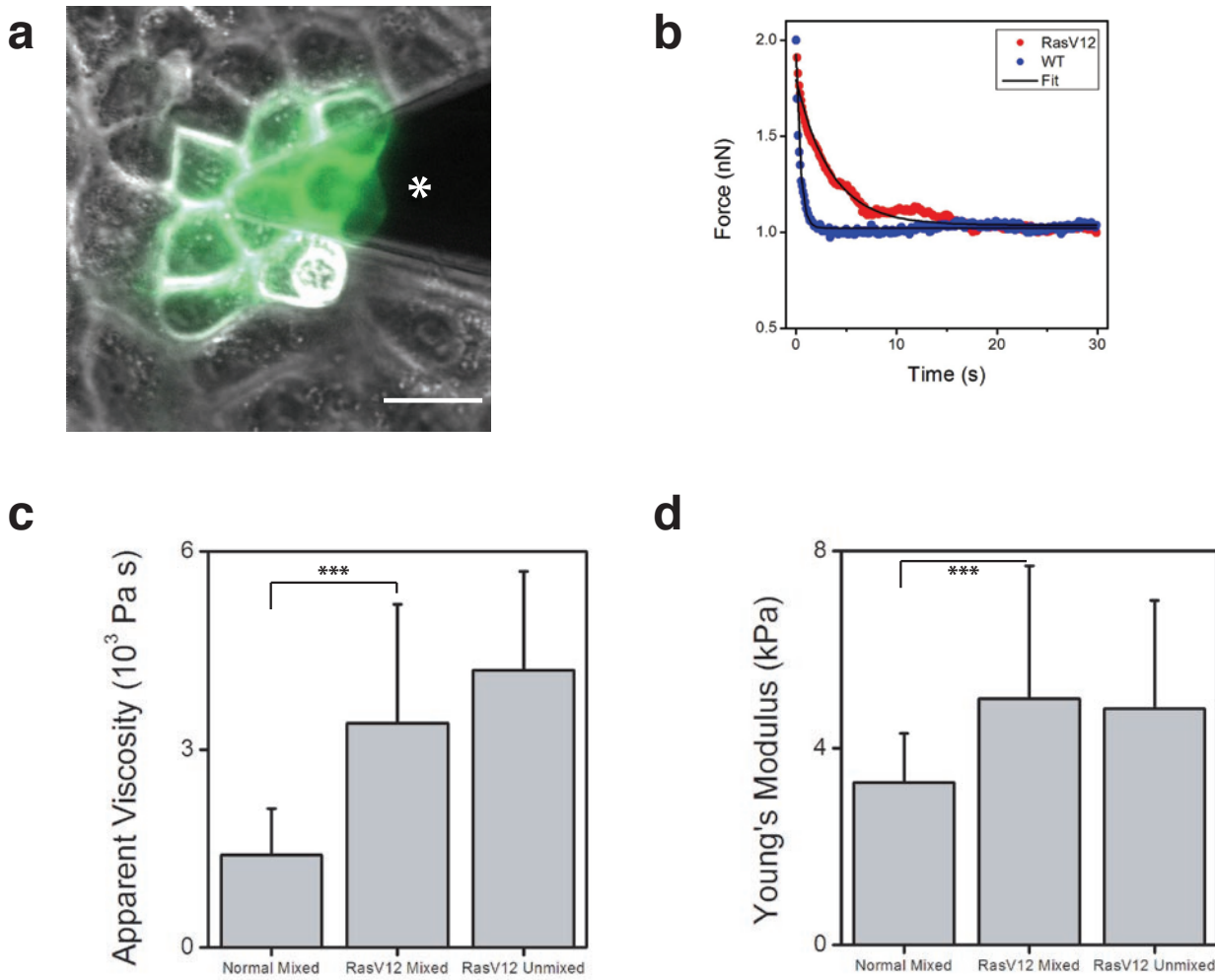


Figure S9 **a** Simultaneous fluorescence and Atomic Force Microscopy (AFM) allows us to directly visualize the AFM tip (*) and measure the mechanical properties of individual RasV12 cells (green) and the surrounding normal cells. Scale bar; 20 μm. **b** Stress-relaxation tests were performed to measure the apparent cell viscosity (μ). RasV12 cells (red) had a much higher μ than normal cells (blue), which resulted in a slower relaxation time after being indented with 2 nN of force. After fitting the data (black) with a stress-relaxation model for AFM, μ values were determined. **c** Normal cells had a μ which was ~2.5 times smaller than RasV12 cells that were mixed or unmixed with normal cells.

Values represent mean \pm s.d. *** $P < 0.0001$. **d** Consistent with these results, the local elasticity of the cell membrane was determined from force-indentation measurements and RasV12 cells were found to be ~1.5 times stiffer than normal cells. Values represent mean \pm s.d. *** $P < 0.0001$. This was also consistent with the relaxed modulus measured from the stress-relaxation tests (data not shown). **c, d** Normal Mixed; normal cells that were mixed with RasV12 cells. RasV12 Mixed; RasV12 cells that were mixed with normal cells. RasV12 Unmixed; RasV12 cells alone. No significant difference was observed between the values of RasV12 cells that were mixed or not mixed with normal cells.

SUPPLEMENTARY INFORMATION

Fig. S1a and S2c

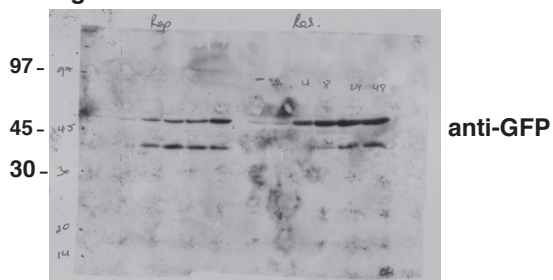


Fig. S1b

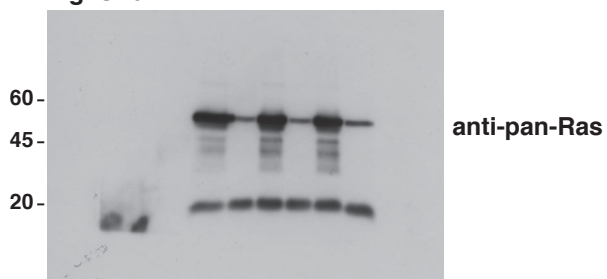


Fig. S1b



Fig. S5e

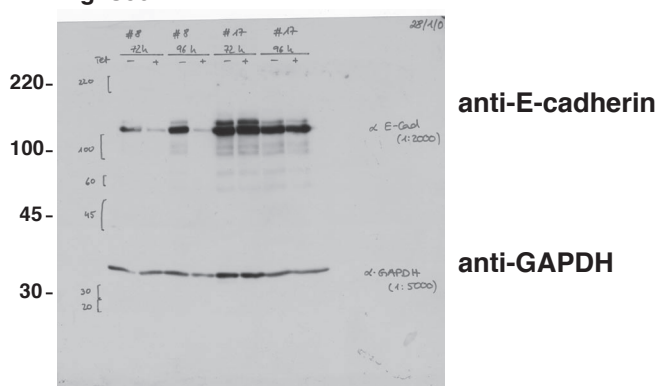


Figure S10 Full scans of western blot data

Supplementary Movies

Movie S1 This movie shows the extrusion of GFP-RasV12 cells from a monolayer of normal MDCK cells, seeded on collagen gels. GFP-RasV12 cells were pre-stained with fluorescent dye and mixed with normal MDCK cells at a ratio of 1:100. Once a monolayer was formed, GFP-RasV12 expression was induced with tetracycline at the beginning of the experiment. Once extruded, the RasV12 cells remain viable and proliferate to form a multi-cellular aggregate that loosely attaches to and moves above the normal MDCK monolayer. Time-lapse images were captured at 10-min intervals for 48 h, with fluorescent images captured every 30 min. (QuickTime; 3 MB)

Movie S2 This movie shows that a GFP-Rap1V12-expressing MDCK cell is not extruded from a monolayer of normal MDCK cells on collagen gels. GFP-Rap1V12 cells were pre-stained with fluorescent dye and mixed with normal MDCK cells at a ratio of 1:100. Once a monolayer was formed, GFP-Rap1V12 expression was induced with tetracycline at the beginning of the experiment. Time-lapse images were captured at 10-min intervals for 24 h, with fluorescent images captured every 30 min. (QuickTime; 2.7 MB)

Movie S3 This movie shows that GFP-RasV12 MDCK cells are not extruded from a monolayer of GFP-RasV12 MDCK cells on collagen gels. GFP-RasV12 cells were pre-stained with fluorescent dye and mixed with non-stained GFP-RasV12 cells at a ratio of 1:100. Once a monolayer was formed, GFP-RasV12 expression was induced with tetracycline at the beginning of the experiment. Time-lapse images were captured at 10-min intervals for 24 h, with fluorescent images captured every 30 min. (QuickTime; 1.2 MB)

Movie S4 This movie shows that a non-extruded GFP-RasV12 cell in a monolayer of normal MDCK cells forms dynamic basal protrusions. GFP-RasV12 cells were pre-stained with fluorescent dye and mixed with normal MDCK cells at a ratio of 1:100. Once a monolayer was formed, GFP-RasV12 expression was induced with tetracycline at the beginning of the experiment. Time-lapse images were captured at 10-min intervals for 24 h, with fluorescent images captured every 50 min. (QuickTime; 136 KB)

Supplementary Discussion

First, we would like to discuss the molecular mechanism of apical extrusion of RasV12 cells. We have not observed F-actin accumulation at the interface between normal and RasV12 cells (Fig. 2a and d), indicating that apical extrusion of RasV12 cells is not induced by “squeezing out” from the surrounding cells as observed in apical extrusion of apoptotic cells¹. The PI3 kinase pathway is involved in lamellipodia formation and PI3K inhibitor does not affect apical extrusion (Fig. 2f), suggesting that apical extrusion is not due to increased migration of RasV12 cells. Then, how are RasV12 cells apically extruded when surrounded by normal cells?

By analysing RasV12 cells that have not yet been extruded and have remained in the monolayer of normal cells, we have found that phosphorylation of myosin light chain is enhanced in RasV12 cells (Fig. 2c; Supplementary Information, Fig. S7b and c) and that F-actin is accumulated at the intercellular junctions between RasV12 cells (Fig. 2a and d; Supplementary Information, Fig. S7f). Activation of myosin-II and intercellular F-actin accumulation would enhance surface tension and cell-cell adhesions of RasV12 cells, respectively². Interestingly, these two parameters have been reported to be involved in cell sorting²⁻⁶; cells with higher surface tension and/or intercellular adhesions are thermodynamically encompassed by cells with lower tension and/or adhesions. Thus, the modulation of cytoskeleton that we have observed in RasV12 cells would promote RasV12 cells to self-aggregate in a monolayer of normal cells as a physically favoured process. We

have also observed that the height of RasV12 cells is enhanced when surrounded by normal cells (Fig. 2a and b), indicating that forces along the apico-basal axis are generated inside RasV12 cells. Since the presence of matrix on the basal side physically blocks basal movement of RasV12 cells, forces toward the apical direction will drive RasV12 cells to be apically extruded.

We have further investigated the physical properties of normal and RasV12 cells by using Atomic Force Microscopy (AFM)(Supplementary Information, Fig. S9). Utilising simultaneous AFM and fluorescence microscopy (Supplementary Information, Fig. S9a), we have directly measured the apparent cell viscosity (μ) and the membrane elasticity (or Young's Modulus)(E) of RasV12 and surrounding normal cells. We have found that RasV12 cells have significantly greater μ (Supplementary Information, Fig. S9b and c) and E values (Supplementary Information, Fig. S9d) than the surrounding normal cells do, indicating that RasV12 cells are stiffer and more viscous than normal cells. These parameters in RasV12 cells in a monolayer of normal cells are not significantly different from those in RasV12 cells in a monolayer of RasV12 cells, suggesting that these physical properties are regulated in a cell-autonomous fashion. Notably, these mechanical parameters are significant in determining cell packing and geometry according to the recently proposed vertex model for cell organisation within an epithelial monolayer⁷. Based on this recent model, we suggest that energetic driving forces may play a vital role in the aggregation (and possibly extrusion) of RasV12 cells within the normal cell monolayer.

In Supplementary Information, Fig. S5, we present our analyses on cell-cell contacts at the interface between RasV12 and non-transformed cells. Components of adherens junctions, E-cadherin, β -catenin and p120-catenin, show incomplete or punctate immunostaining at cell-cell contacts where RasV12 cells extend a protrusion (Supplementary Information, Fig. S5a-c; data not shown for p120). Frequently, E-cadherin and β -catenin localise in vesicular puncta within the protrusion (Supplementary Information, Fig. S5d; data not shown for β -catenin). Localisation of tight junction protein ZO-1 is not affected by protrusion formation (Supplementary Information, Fig. S5a and b, white arrowheads), indicating that E-cadherin-based cell-cell contacts are specifically disrupted. Both adherens junctions and tight junctions are maintained between RasV12 cells (Supplementary Information, Fig. S5a and b, white arrows), suggesting that loss of E-cadherin-based cell-cell adhesion specifically occurs at the interface between RasV12 and non-transformed cells. We therefore ask whether loss of E-cadherin is sufficient to induce protrusion formation by knocking down E-cadherin protein in MDCK cells using a tetracycline-inducible shRNA system (Supplementary Information, Fig. S5e). No protrusion formation is observed at the interface between normal and E-cadherin-deficient MDCK cells (Supplementary Information, Fig. S5f), indicating that loss of E-cadherin alone does not lead to protrusion formation but additional Ras-mediated signalling is required.

We show in Fig. 4c that ROCK and Cdc42 are crucial in determining the fate of RasV12 cells in a monolayer of normal cells; either apically extruded, or

remaining in the monolayer and forming basal protrusions. Expression of dominant negative ROCK suppresses RasV12-induced phosphorylation of myosin light chain (Supplementary Information, Fig. S7b and c), suggesting its role in activation of myosin-II. However, we cannot exclude the possibility that other pathways may also be involved in the regulation of myosin-II. ROCK can be activated by active Rho⁸⁻¹⁰. Interestingly, expression of p50RhoGAP, an inactivator of Rho¹¹, significantly enhances apical extrusion of RasV12 cells (Supplementary Information, Fig. S7d), suggesting that some Rho downstream targets play a negative role in this process. It is feasible that Rho activity may be regulated locally or temporally, which affects its multiple downstream targets and the fate of RasV12 cells. In future studies, it remains to be clarified how the activity of ROCK and Cdc42 is regulated in RasV12 cells surrounded by normal cells.

E-cadherin knockdown in cells surrounding RasV12 cells reduces the frequency of apical extrusion, while promoting basal protrusion formation and invasion (Fig. 5a-c). In addition, other data suggest that signalling pathways of surrounding normal cells can affect the behaviour of RasV12 cells. Expression of dominant negative Raf has no effect on the frequency of basal protrusion formation of RasV12 cells in a monolayer of normal cells (Fig. 4b), whereas addition of MEK inhibitor suppresses it (Fig. 3e). Expression of dominant negative ROCK substantially promotes protrusion formation of RasV12 cells (Fig. 4c), whereas addition of blebbistatin does not affect it (Fig. 3e). These data

indicate the involvement of basal activity of MEK and myosin-II of surrounding normal cells in this process. Collectively, our results suggest that the fate of RasV12 cells in a monolayer of normal cells is determined by the total balance of multiple signalling pathways in both RasV12 cells and surrounding normal cells. It is highly plausible that apical extrusion would suppress tumour formation and that basal protrusion formation and basal delamination would promote it. We expect that novel therapeutic treatment for cancer may be discovered by further studying the molecular mechanisms of apical extrusion and basal protrusion formation of transformed cells.

Finally, in MDCK cells, we have found that expression of v-Src highly promotes apical cell extrusion (Supplementary Information, Fig. S8), but not basal protrusion formation (data not shown). Apical extrusion is observed in cells expressing either RasV12 or v-Src that stimulate distinct downstream targets. Therefore, it will be interesting to investigate whether common signalling pathways are involved in these processes. Overexpression of Myc induces neither apical extrusion nor basal protrusion formation (Supplementary Information, Fig. S8, and data not shown). These data suggest that different oncogenic stimuli induce different phenomena between normal and transformed cells, as previously shown in *Drosophila melanogaster*^{12, 13}. In future studies, it should be examined whether deregulation of other oncoproteins or tumour suppressor proteins induces distinct phenomena at the interface with normal cells and how those phenomena are involved in the early stage of carcinogenesis in vertebrates.

Supplementary Methods

Plasmids. pcDNA/TO/GFP was constructed as described previously¹⁴. cDNAs of H-RasV12 and Rap1V12 were amplified by PCR from pRK5-myc-H-RasV12 and pRK5-myc-Rap1V12 respectively, and were then cloned into an EcoRI site of pcDNA/TO/GFP. Similarly, cDNA of c-myc was amplified by PCR from MSCV-hmyc-IRES-GFP, and cloned into EcoRI/Xho sites of pcDNA/TO/GFP.

pcDNA6/TR and pcDNA4/TO were obtained from Invitrogen. pRK5-myc-H-RasV12, pRK5-myc-Rap1V12, pRK5-myc-Cdc42N17, pRK5-myc-Cdc42L61, pBOS-myc-Rac1N17, pBOS-myc-Rac1V12, pBOS-myc-RhoV14, and pGEX-2T-p50RhoGAP catalytic domain were all kindly provided by A. Hall (Memorial Sloan-Kettering Cancer Center, NY). pLXSN-myc-p110-CAAX was kindly provided by A. Lloyd (University College London, London). MSCV-hmyc-IRES-GFP was provided by S. Lowe (Cold Spring Harbor Laboratory, NY). pEGFP, pCMV-Raf-CAAX and pCMV-RafS621A were from Clontech (Mountain View, CA). pCAGGS-myc-ROCK1 Δ3 KD (ROCK-DN) was kindly provided by E. Sahai (Cancer Research UK, London). To construct pcDNA/TO/Cherry p50RhoGAP catalytic domain, the cDNA of p50RhoGAP catalytic domain was amplified from pGEX-2T-p50RhoGAP catalytic domain by PCR, and inserted into the EcoRI/NotI site of pcDNA/TO/Cherry. To obtain pcDNA/TO/Cherry, the cDNA of mCherry was amplified from pmCherry C1 by PCR, and was inserted into the EcoRI/BamHI site of pcDNA/TO. pmCherry C1 was a generous gift from

R. Y. Tsien (University of California at San Diego, CA). pSG-v-Src was described previously¹⁵.

Cell culture and RNA interference. MDCK cells were cultured in Dulbecco's modified Eagle's medium (DMEM) supplemented with 10% fetal calf serum (FCS) and penicillin/streptomycin at 37°C and ambient air supplemented with 5% CO₂. To establish MDCK cells stably expressing GFP-RasV12 in an inducible manner, a Tet-ON system was used. Briefly, MDCK cells were transfected with pcDNA6/TR using LipofectamineTM 2000 (Invitrogen), followed by selection in medium containing 5 µg ml⁻¹ of blasticidin (Invitrogen). pcDNA4/TO/GFP-RasV12 was then used for the second transfection and the doubly transfected cells were selected in medium containing 10% FCS (tetracycline-free) (PAA Laboratories, Pasching, Austria), 5 µg ml⁻¹ of blasticidin and 400 µg ml⁻¹ of zeocin (Invitrogen). MDCK cells stably expressing GFP and GFP-Rap1V12 were produced under the same conditions. To induce GFP, GFP-RasV12 and GFP-Rap1V12 expression, 2 µg ml⁻¹ tetracycline was added to culture medium. After the establishment of the RasV12 cell line, we confirmed that the expression level of GFP-RasV12 was uniform between cells as follows; we plated RasV12 cells sparsely and established more than 30 independent clones isolated from single cells. By comparing the expression of GFP-RasV12 between the clones by

Western blotting, we confirmed that GFP-RasV12 is indeed expressed at the same level in the RasV12 cell line we have used for the experiments.

For transient expression experiments (Fig. 4a-c; Supplementary Information, Fig. S6-8), MDCK cells were first seeded on collagen-coated coverslips in 6-well culture dishes (Nunc, Roskilde, Denmark) at a density of 7×10^5 cells per well. On the following day, cells were transiently transfected with the indicated constructs (2 μ g per construct) using LipofectamineTM 2000 (Invitrogen) according to manufacturer's instructions. After 24 h of transfection, cells were fixed and immunostained as described below. In Supplementary Information, Fig. S7a, following 4 hr of transfection, MDCK cells transiently transfected with constitutively active Rho (Myc-RhoV14) were further incubated with or without Y27632 for 18 h.

MDCK cells stably expressing E-cadherin shRNA in a tetracycline-inducible manner were produced as follows; E-cadherin shRNA oligonucleotides (E-Cad shRNA-1; 5'-

GATCCCCGGACGTGGAAGATGTGAATTCAAGAGAATTCACATCTTCC

ACGTCCTTTGGAAA-3' and 5'-

AGCTTTCCAAGGACGTGGAAGATGTGAATTCTCTTGAAATTAC

ATCTTCCACGTCCGGG-3', and E-Cad shRNA-2;

5'GATCCCCGTCTAACAGGGACAAAGAATTCAAAGAGATTCTTGTCCC

TGTTAGACTTTTC-3' and 5'-

TCGAGAAAAAGTCTAACAGGGACAAAGAATCTCTGAATTCTTGCC

CTGTTAGACGGG-3')¹⁶ were cloned into BglII and XhoI sites of pSUPERIOR.neo+gfp (Oligoengine, Seattle, WA). MDCK-pTR cells were transfected with pSUPERIOR.neo+gfp E-cadherin shRNA using MetafecteneTMPro (Biontex, Germany), followed by selection in medium containing 5 µg ml⁻¹ of blasticidin and 800 µg ml⁻¹ of G418 (Calbiochem). More than two stable clones were obtained for two independent shRNA oligonucleotides. Knockdown of E-cadherin was analysed by immunofluorescence and Western blotting following 96 h incubation with tetracycline (2 µg ml⁻¹). It should be noted that comparable effect of E-cadherin knockdown on protrusion formation or apical extrusion was observed in cells expressing E-cadherin shRNA-1 or -2.

Cells were plated as described below, except where indicated as low-density cells were plated at 1 x 10⁵ cells in 6-well culture dishes.

Immunofluorescence. Immunofluorescence of cells cultured on serum-coated glass coverslips was performed as previously described¹⁷. Cells cultured on collagen gels were examined using a Leica TCS SPE confocal microscope and Leica Application Suite (LAS) software. Cells cultured on glass coverslips were examined using a Bio-Rad Radiance 2100 MP system mounted on a Nikon 800 microscope using Lasersharp software (Biorad). Images were analysed using ImageJ 1.36b (National Institute of Health) or Volocity software (Improvision).

Cell height (from apical to basal membranes) and F-actin accumulation at cell-cell contacts were both quantified using Metamorph 6.0 digital analysis software (Universal Imaging)(Fig. 2b and d; Supplementary Information, Fig. S7e and f). To determine the level of F-actin at cell-cell contacts, a defined region was created to encompass the area of a cell-cell contact in xz confocal sections. The total pixel intensity within this region (200 pixels) was determined. For quantification of apical extrusion of GFP-RasV12 cells in the presence or absence of inhibitors (Fig. 2f), GFP-RasV12 cells in groups > 3 cells were examined. Minor and major protrusions were counted as less or greater than 10 μ m in length, respectively (Fig. 3d). To determine the amount of GST-WASP-CRIB (Fig. 4e) or p-MLC (Supplementary Information, Fig. S7c) in GFP- or GFP-RasV12-expressing cells, Metamorph 6.0 digital analysis software (Universal Imaging) was used. Briefly, a defined region was created in the cytoplasm of the indicated cells in xz confocal sections. For each cell, 5 (for GST-WASP-CRIB) or 8 (for p-MLC) regions were created. The total pixel intensity within each region (73 pixels) was determined and the mean pixel intensity was calculated for each cell. In Fig. 5c, GFP-RasV12 cells or normal MDCK cells that were apically extruded, basally delaminated or formed basal protrusions were counted and expressed as a ratio relative to total cells. Cells were counted following 24 h of tetracycline addition, however MDCK-pTR E-cadherin shRNA cells were incubated with tetracycline for 72 h prior to mixing with other cells to induce sufficient knockdown of E-cadherin protein. In Supplementary Information, Fig. S5c, the correlation between protrusion

formation and E-cadherin or β -catenin mis-localisation was quantified as follows.

Cell-cell contacts between RasV12 and normal MDCK cells were first identified using F-actin staining at the contact site. When 50% or less of the contact site was stained with E-cadherin or β -catenin, it was counted as broken or punctate.

Conversely, cell-cell contacts with $> 80\%$ E-cadherin or β -catenin staining were counted as linear.

Atomic Force Microscopy. A JPK AFM (Nanowizard I) was used for all experiments with MSCT-AUHW cantilevers (14 ± 1 pN/nm). The AFM was mounted on an inverted Olympus IX71 phase contrast and fluorescence microscope for simultaneous optical imaging and mechanical analyses. Force curves were measured at 1 Hz and analysed with the Hertz model to determine cortical elasticity for a 500-nm indentation¹⁸. Stress-relaxation experiments were performed in constant height mode and the vertical deflection sampled at 10 Hz. Data were fit with a stress-relaxation model (in the limit of a conical indenter) according to previous methodologies^{19,20} to determine the apparent viscosity of the cell.

Statistical analyses. Student's *t* tests were used to determine P value because this test requires variables with no fixed limits.

Fig. 1d: ratios were transformed to arcsin using Excel software, and two-tailed Student's *t* tests were used to determine P value. Control, n = 98 groups of cells; + 4-AP, n = 101 groups of cells. Values represent mean \pm s.d. P = 0.31. Fig. 2b: two-tailed Student's *t* tests were used to determine P value. Values represent mean \pm s.d. A total of 40-85 cells from three independent experiments were analysed. MDCK vs GFP-RasV12, ***P = 0.00036; GFP-RasV12 vs GFP-RasV12 cells only, ***P = 0.00018. Fig. 2d: two-tailed Student's *t* tests were used to determine P value. Values represent mean \pm s.d. A total of 30-60 cell-cell contacts from four independent experiments were analysed. R:R vs R:M, ***P = 1.3×10^{-14} ; R:R vs M:M, ***P = 1.2×10^{-17} ; R:R vs R:R (RasV12 cells only), ***P = 8.0×10^{-9} . Fig. 2f: the number of RasV12 cell aggregates in which the majority or minority of RasV12 cells were apically extruded was expressed as a ratio relative to that of total RasV12 cell aggregates. RasV12 cells in groups > 3 cells were included in analyses, and one-tailed Student's *t* tests were used to determine P value to compare with DMSO control. In each experiment, ~ 20 groups of RasV12-expressing cells were counted. Values represent mean from 4-5 independent experiments \pm s.d. U0126, ***P = 0.00016 for white bar and 2.3×10^{-6} for black bar; Y27632, **P = 0.0041 for white bar and P = 0.11 for black bar; blebbistatin, ***P = 0.00022 for white bar and **P = 0.0012 for black bar; cytochalasin D, ***P = 0.00010 for white bar and *P = 0.026 for black bar. Fig. 3d: ratios were transformed to arcsin using Excel software and two-tailed Student's *t* tests were used to determine P value. Minor or major protrusion formation at cell-cell

contacts, relative to total cell-cell contacts was scored between RasV12 and normal MDCK cells ($n= 230$) or between RasV12 cells ($n= 180$). Values represent mean \pm s.d. $***P = 4.4 \times 10^{-5}$. Fig. 3e: one-tailed Student's *t* tests were used to determine P value to compare with DMSO control. 60-80 groups of cells were analysed for each experimental condition. Values represent mean from 3-4 independent experiments \pm s.e.m. U0126, * $P = 0.016$; LY294002, * $P = 0.0070$; cytochalasin D, ** $P = 0.0031$. Fig. 4a and b: the number of GFP or GFP-RasV12 cells apically extruded or forming major basal protrusions was expressed as a ratio relative to that of total cells. Two-tailed Student's *t* tests were used to determine P value. In each experiment, 50-150 cells were counted. Values represent mean from more than five independent experiments \pm s.e.m. Fig. 4a, $***P = 1.1 \times 10^{-7}$ for white bar and $***P = 0.00099$ for black bar. Fig. 4b, $***P = 9.9 \times 10^{-5}$ for white bar. Fig. 4c: the number of GFP or GFP-RasV12 cells apically extruded or forming major basal protrusions was expressed as a ratio relative to that of total cells. Two-tailed Student's *t* tests were used to determine P value. In each experiment, 50-115 cells were counted. Values represent mean from more than five independent experiments \pm s.e.m. GFP-RasV12 vs Cdc42N17 + GFP-RasV12, $***P = 1.2 \times 10^{-7}$ for white bar and $***P = 4.1 \times 10^{-8}$ for black bar; GFP-RasV12 vs ROCK-DN + GFP-RasV12, ** $P = 3.7 \times 10^{-7}$ for white bar and ** $P = 0.0014$ for black bar. Fig. 4e: two-tailed Student's *t* tests were used to determine P value. A total of 50-70 cells from three independent experiments were analysed. Values represent mean \pm s.e.m. ** $P = 0.0019$ and $***P = 2.7 \times 10^{-8}$. Fig. 5c: one-

tailed Student's *t* tests were used to determine P value. Values represent mean from 2-3 independent experiments \pm s.d. GFP-RasV12 + E-cadherin shRNA cells, n = 301 cells; MDCK + E-cadherin shRNA cells, n = 396 cells; GFP-RasV12 + MDCK cells, n = 536 cells. *P = 0.040, **P = 0.0026, ***P = 0.00044. Fig. S5c: one-tailed Student's *t* tests were used to determine P values. Values represent mean \pm s.d. n = 54 for both E-cadherin and β -catenin. *P = 0.012 for E-cadherin and *P = 0.041 for β -catenin. Fig. S7c: two-tailed Student's *t* tests were used to determine P value. A total of 25-50 cells from three independent experiments were analysed. Values represent mean \pm s.e.m. **P = 0.0023 and ***P = 6.4 x 10⁻⁹. Fig. S7d: the number of GFP or GFP-RasV12 cells apically extruded or forming major basal protrusions was expressed as a ratio relative to that of total cells. Two-tailed Student's *t* tests were used to determine P value. In each experiment, 50-150 cells were counted. Values represent mean from more than five independent experiments \pm s.e.m. GFP-RasV12 vs Rac1N17+GFP-RasV12, P = 0.62 for white bar, P = 0.98 for black bar; GFP-RasV12 vs RhoGAP+GFP-RasV12, P = 0.037 for white bar, P = 0.81 for black bar. Fig. S7e: two-tailed Student's *t* tests were used to determine P value. Values represent mean \pm s.d. A total of 30-160 cells from five independent experiments were analysed. GFP vs GFP-RasV12, ***P = 1.7 x 10⁻²⁰; GFP-RasV12 vs Cdc42N17+GFP-RasV12, ***P = 4.7 x 10⁻¹⁷; GFP-RasV12 vs ROCK-DN+GFP-RasV12, ***P = 6.7 x 10⁻⁵. Fig. S7f: two-tailed Student's *t* tests were used to determine P value. Values represent mean \pm s.d. A total of 25-60 cells from four independent experiments were analysed. GFP vs GFP-RasV12,

***P = 1.3 x 10⁻¹³; GFP-RasV12 vs Cdc42N17+GFP-RasV12, ***P = 9.8 x 10⁻⁶;
GFP-RasV12 vs ROCK-DN+GFP-RasV12, ***P = 3.2 x 10⁻⁸. Fig. S9: two-tailed
Student's *t* tests were used to determine P values. Values represent mean from two
independent experiments \pm s.d. Normal mixed vs RasV12 mixed ***P = 8.6 X 10⁻⁵
for apparent viscosity (n = 16), ***P = 1.2 X 10⁻⁷ for Young's Modulus (n = 15).

References

1. Rosenblatt, J., Raff, M. C. & Cramer, L. P. An epithelial cell destined for apoptosis signals its neighbors to extrude it by an actin- and myosin-dependent mechanism. *Curr Biol* **11**, 1847-57 (2001).
2. Lecuit, T. & Lenne, P. F. Cell surface mechanics and the control of cell shape, tissue patterns and morphogenesis. *Nat Rev Mol Cell Biol* **8**, 633-44 (2007).
3. Hayashi, T. & Carthew, R. W. Surface mechanics mediate pattern formation in the developing retina. *Nature* **431**, 647-52 (2004).
4. Foty, R. A., Pfleger, C. M., Forgacs, G. & Steinberg, M. S. Surface tensions of embryonic tissues predict their mutual envelopment behavior. *Development* **122**, 1611-20 (1996).
5. Steinberg, M. S. & Takeichi, M. Experimental specification of cell sorting, tissue spreading, and specific spatial patterning by quantitative differences in cadherin expression. *Proc Natl Acad Sci U S A* **91**, 206-9 (1994).
6. Krieg, M. et al. Tensile forces govern germ-layer organization in zebrafish. *Nat Cell Biol* **10**, 429-36 (2008).
7. Farhadifar, R., Roper, J. C., Aigouy, B., Eaton, S. & Julicher, F. The influence of cell mechanics, cell-cell interactions, and proliferation on epithelial packing. *Curr Biol* **17**, 2095-104 (2007).
8. Watanabe, G. et al. Protein kinase N (PKN) and PKN-related protein rhophilin as targets of small GTPase Rho. *Science* **271**, 645-8 (1996).
9. Amano, M. et al. Identification of a putative target for Rho as the serine-threonine kinase protein kinase N. *Science* **271**, 648-50 (1996).
10. Sahai, E. & Marshall, C. J. ROCK and Dia have opposing effects on adherens junctions downstream of Rho. *Nat Cell Biol* **4**, 408-15 (2002).
11. Lancaster, C. A. et al. Characterization of rhoGAP. A GTPase-activating protein for rho-related small GTPases. *J Biol Chem* **269**, 1137-42 (1994).
12. Moreno, E. Is cell competition relevant to cancer? *Nat Rev Cancer* **8**, 141-7 (2008).
13. Diaz, B. & Moreno, E. The competitive nature of cells. *Exp Cell Res* **306**, 317-22 (2005).

14. Dupre-Crochet, S. et al. Casein kinase 1 is a novel negative regulator of e-cadherin-based cell-cell contacts. *Mol Cell Biol* **27**, 3804-16 (2007).
15. Fujita, Y. et al. Hakai, a c-Cbl-like protein, ubiquitinates and induces endocytosis of the E-cadherin complex. *Nat Cell Biol* **4**, 222-31 (2002).
16. Capaldo, C. T. & Macara, I. G. Depletion of E-cadherin disrupts establishment but not maintenance of cell junctions in Madin-Darby canine kidney epithelial cells. *Mol Biol Cell* **18**, 189-200 (2007).
17. Hogan, C. et al. Rap1 regulates the formation of E-cadherin-based cell-cell contacts. *Mol Cell Biol* **24**, 6690-700 (2004).
18. Matzke, R., Jacobson, K. & Radmacher, M. Direct, high-resolution measurement of furrow stiffening during division of adherent cells. *Nat Cell Biol* **3**, 607-10 (2001).
19. Darling, E. M., Topel, M., Zauscher, S., Vail, T. P. & Guilak, F. Viscoelastic properties of human mesenchymally-derived stem cells and primary osteoblasts, chondrocytes, and adipocytes. *J Biomech* **41**, 454-64 (2008).
20. Darling, E. M., Zauscher, S., Block, J. A. & Guilak, F. A thin-layer model for viscoelastic, stress-relaxation testing of cells using atomic force microscopy: do cell properties reflect metastatic potential? *Biophys J* **92**, 1784-91 (2007).